Enhanced tyrosine hydroxylase activity induces oxidative stress, causes accumulation of autotoxic catecholamine metabolites, and augments amphetamine effects in vivo.

Laura M Vecchio

Patricia Sullivan

Amy R Dunn

Marie Kristel Bermejo

Rong Fu

See next page for additional authors

Authors

Laura M Vecchio, Patricia Sullivan, Amy R Dunn, Marie Kristel Bermejo, Rong Fu, Shababa T Masoud, Emil Gregersen, Nikhil M Urs, Reza Nazari, Poul Henning Jensen, Amy Ramsey, David S Goldstein, Gary W Miller, and Ali Salahpour

ORIGINAL ARTICLE

Enhanced tyrosine hydroxylase activity induces oxidative stress, causes accumulation of autotoxic catecholamine metabolites, and augments amphetamine effects in vivo

Laura M. Vecchio[1] | Patricia Sullivan[2] | Amy R. Dunn[3] | Marie Kristel Bermejo[1] | Rong Fu[4] | Shababa T. Masoud[1] | Emil Gregersen[5] | Nikhil M. Urs[6] | Reza Nazari[1] | Poul Henning Jensen[5] | Amy Ramsey[1] | David S. Goldstein[2] | Gary W. Miller[7] | Ali Salahpour[1]

[1]Department of Pharmacology and Toxicology, Faculty of Medicine, University of Toronto, Toronto, ON, Canada

[2]Autonomic Medicine Section, Clinical Neurosciences Program, Division of Intramural Research, National Institute of Neurological, Disorders and Stroke, National Institutes of Health, Bethesda, MD, USA

[3]The Jackson Laboratory. Bar Harbor, Maine, USA

[4]Department of Pharmacology, Emory University School of Medicine, Atlanta, GA, USA

[5]Danish Research Institute of Translational Neuroscience – DANDRITE, Department of Biomedicine, Faculty of Health, Aarhus University, Aarhus C., Denmark

[6]Department of Pharmacology and Therapeutics, University of Florida, Gainsville, FL, USA

[7]Department of Environmental Health Sciences, Mailman School of Public Health, Columbia University Medical Centre, New York, NY, USA

Correspondence
Ali Salahpour, Department of Pharmacology and Toxicology, Faculty of Medicine, University of Toronto. Toronto, ON M5S 1A8, Canada.
Email: ali.salahpour@utoronto.ca

Abstract

In Parkinson's disease, dopamine-containing nigrostriatal neurons undergo profound degeneration. Tyrosine hydroxylase (TH) is the rate-limiting enzyme in dopamine biosynthesis. TH increases in vitro formation of reactive oxygen species, and previous animal studies have reported links between cytosolic dopamine build-up and oxidative stress. To examine effects of increased TH activity in catecholaminergic neurons in vivo, we generated TH-over-expressing mice (TH-HI) using a BAC-transgenic approach that results in over-expression of TH with endogenous patterns of expression. The transgenic mice were characterized by western blot, qPCR, and immunohistochemistry. Tissue contents of dopamine, its metabolites, and markers of oxidative stress were evaluated. TH-HI mice had a 3-fold increase in total and

Abbreviations: AADC, aromatic amino acid decarboxylase; ALDH, aldehyde dehydrogenase; BAC, bacterial artificial chromosome; BCA, bicinchoninic acid; BME, beta-mercaptoethanol; CAMKII, calmodulin-stimulated protein kinase II; CT, cycle threshold; Cys-DA, cysteinylated dopamine; Cys-DOPA, cysteinylated dihydroxyphenylalanine; DA, dopamine; DA-Q, dopamine quinone; DAT, dopamine transporter; DHPG, dihydroxyphenylglycine; DOPAC, 3,4-dihydroxyphenylacetic acid; DOPAL, 3,4-dihydroxyphenylacetaldehyde; DOPA-Q, dihydroxyphenylalanine quinone; ERK, extracellular signal-related protein kinases; GAPDH, glyceraldehyde 3-phosphate dehydrogenase; GSH, glutathione; H_2O_2, hydrogen peroxide; HPLC, high performance liquid chromatography; LB, lysogeny broth; L-DOPA, L-3,4-dihydroxyphenylalanine; MAO, monoamine oxidase A; MES, 2[N-morpholino] ethanesulphonic acid; MOPS, 3-(N-morpholino)propanesulfonic acid; MPA, metaphosphoric acid; MPTP, 1-methyl-4-phenyl-1,2,3,6-tetrahydropyridine; NA, noradrenaline; NET, norepinephrine (or noradrenaline) transporter; PBS, phosphate buffered saline; PCR, polymerase chain reaction; PKA, cyclic AMP-dependent protein kinase A; Pkg, cGMP-dependent protein kinase (or protein kinase G); PP2A, protein phosphatase 2A; PVDF, polyvinylidene difluoride; qPCR, quantitative polymerase chain reaction; RIPA, radioimmunoprecipitation assay; ROS, reactive oxygen species; SDS, sodium dodecyl sulfate; Ser-, serine; TEAM, triethanolamine; Tfrc, transferrin receptor; TH, tyrosine hydroxylase; VMAT2, vesicular monoamine transporter-2.

phosphorylated TH levels and an increased rate of dopamine synthesis. Coincident with elevated dopamine turnover, TH-HI mice showed increased striatal production of H_2O_2 and reduced glutathione levels. In addition, TH-HI mice had elevated striatal levels of the neurotoxic dopamine metabolites 3,4-dihydroxyphenylacetaldehyde and 5-S-cysteinyl-dopamine and were more susceptible than wild-type mice to the effects of amphetamine and methamphetamine. These results demonstrate that increased TH alone is sufficient to produce oxidative stress in vivo, build up autotoxic dopamine metabolites, and augment toxicity.

KEYWORDS

amphetamine, DOPAL, dopamine, oxidative stress, tyrosine hydroxylase

1 | INTRODUCTION

The neurochemical hallmark of Parkinson's disease is depletion of the catecholamine dopamine in the nigrostriatal system, particularly in the putamen (Kish et al. 1988). By the time the characteristic motor symptoms manifest clinically, it is likely that a substantial proportion of striatal dopaminergic terminals have already been lost (Dalle-Donne et al. 2008). The dropout of midbrain substantia nigra neurons seems often to be preceded by comparable degeneration of noradrenergic neurons in the pontine locus coeruleus (Del Tredici & Braak, 2013), which might contribute to pre-motor symptoms (Braak et al. 2003; Darvas et al. 2014; Fahn, 2003).

Oxidative stress is widely recognized as a contributor to the pathogenesis of idiopathic Parkinson's disease; however, why catecholaminergic neurons are especially susceptible remains incompletely understood. Many factors may underlie the preferential vulnerability of catecholamine neurons, including patterns of alpha(α)-synuclein aggregation and spread; mitochondrial dysfunction; an extensive axonal arbor, particularly characteristic of substantia nigra cells; and cell- or region-specific characteristics of cell signalling, including an increasing dependency on calcium channels, which can increase mitochondrial stress (Blesa et al. 2015; Bolam & Pissadaki, 2012; Puspita et al. 2017; Ricke et al. 2020; Surmeier, 2007, 2018; Surmeier et al. 2017). Another specific source of vulnerability may relate to autotoxicity resulting from metabolites of the catecholamines (Goldstein et al. 2014; Masato et al. 2019; Miyazaki & Asanuma, 2008). Testing this notion in vivo, however, has been a difficult challenge that few studies have tackled.

The rate-limiting enzyme in catecholamine biosynthesis is tyrosine hydroxylase (TH). During catecholamine synthesis, small amounts of reactive oxygen species (ROS) are generated (Adams et al. 1997; Haavik et al. 1997; Kostyn et al. 2020). Activity of TH is modulated by phosphorylation of 3 main serine (Ser-) residues on its amino terminus: Ser19, Ser31, and Ser40 (Daubner et al. 2011; Dunkley & Dickson, 2019). The predominant source of TH activation is phosphorylation at Ser40, chiefly mediated by cyclic AMP-dependent protein kinase A (PKA) (Lehmann et al. 2006; Salvatore et al. 2001). Phosphorylation of TH at Ser31 by extracellular signal-related protein

kinases I and II (ERKI and II) is also believed to directly promote enzymatic activity, possibly with a greater role in somatodendritic compartments of dopaminergic cells (Salvatore, 2014; Salvatore et al. 2016, 2018). In contrast, phosphorylation of Ser19, primarily mediated by calmodulin-stimulated protein kinase II (CaMK II), is believed to facilitate enzymatic activity indirectly by inducing a conformational change and increasing phosphorylation at Ser40 and Ser31 (Haycock et al. 1998; Lindgren et al. 2000). By releasing the enzyme from end-point inhibition and returning it to its activate state, phosphorylation of TH plays a direct role in the rate of catecholamine synthesis and bioavailability (Daubner et al. 2011; Dunkley et al. 2004).

Protein phosphatase 2A (PP2A) is the main phosphatase responsible for dephosphorylating TH and regulating its activity (Haavik et al. 1989; Peng et al. 2005). In addition, α-synuclein also negatively regulates the activity of TH, directly and indirectly, by activating PP2A (Hua et al. 2015; Liu et al. 2008; Peng et al. 2005; Perez et al. 2002; Qu et al. 2018). However, α-synuclein phosphorylated at Ser129—a major constituent of insoluble α-synuclein aggregates (Arawaka et al. 2017; Walker et al. 2013; Zhou et al. 2011)—has a limited ability to inhibit TH activity (Lou et al. 2010; Wu et al. 2011) and has been linked to dopamine dysregulation (Alerte et al. 2008). Increased levels of Ser129 phosphorylation have been associated with diminished PP2A, in part because PP2A is also responsible for dephosphorylating α-synuclein (Liu et al. 2015; Park et al. 2016). Recent studies have shown that the relationship between reduced PP2A and α-synuclein Ser129 phosphorylation is one of positive feedback, with aggregated or phosphorylated α-synuclein further reducing PP2A function (Chen et al. 2016; Liu et al. 2015; Tian et al. 2018) and TH regulation (Farrell et al. 2014).

Studies in transgenic models show that increased TH activity and elevated ROS can result from diminished regulation placed on the enzyme. In *Drosophilia* and *C. elegans*, dysfunctional α-synuclein has been reported to increase levels of phosphorylated TH and elevate dopamine levels, ultimately leading to oxidative stress and neurodegeneration (Locke et al. 2008; Park et al. 2007). Similarly, mice with mutated or aggregated α-synuclein show increased levels of TH activity and behavioural impairment attributed to catecholamine dysregulation (Alerte et al. 2008; Farrell et al. 2014). Therefore,

increased activity of TH, in concert with other changes, could present a source of oxidative stress unique to catecholamine neurons (Alerte et al. 2008; Chen et al. 2016; Hua et al. 2015; Liu et al. 2015; Lou et al. 2010; Park et al. 2016; Peng et al. 2005).

ROS resulting from the accumulation of cytosolic dopamine may represent an additional source of oxidative stress in cells with increased synthetic activity (Chen et al. 2008; Stansley & Yamamoto, 2013). Ordinarily, cytosolic dopamine levels are kept very low because of avid uptake into vesicles via the type 2 vesicular monoamine transporter (VMAT2). Unsequestered dopamine undergoes metabolism by monoamine oxidase (MAO), which generates hydrogen peroxide (H_2O_2) as well as the catecholaldehyde 3,4-dihydroxyphenylacetaldehyde (DOPAL), a highly reactive intermediate metabolite (Goldstein et al. 2016; Graham, 1978; Hermida-Ameijeiras et al. 2004). DOPAL is metabolized by aldehyde dehydrogenase (ALDH) to form 3,4-dihydroxyphenylacetic acid (DOPAC), which rapidly exits the cells (Lamensdorf et al. 2000).

According to the catecholaldehyde hypothesis, DOPAL can play a role in the pathogenesis of Parkinson's disease (Casida et al. 2014; Fitzmaurice et al. 2013; Goldstein et al. 2016; Panneton et al. 2010; Wey et al. 2012), especially via modifications of cytosolic proteins such as α-synuclein (Jinsmaa et al. ,2018, 2020). DOPAL has been shown to promote oligomerization of α-synuclein by covalent modifications of lysine residues (Burke et al. 2008; Follmer et al. 2015), and DOPAL-induced α-synuclein oligomers impede vesicular functions (Plotegher et al. 2017), potentially setting the stage for a vicious pathophysiological cycle. Moreover, in the setting of divalent metal cations, DOPAL can react with H_2O_2 to produce extremely toxic hydroxyl radicals (Li et al. 2001; Werner-Allen et al. 2017). Finally, DOPAL spontaneously oxidizes to DOPAL-quinone, in the process generating superoxide radicals (Anderson et al. 2011; Werner-Allen et al. 2017).

Cytosolic dopamine can also undergo spontaneous oxidation to produce dopamine-quinone and then a variety of potentially toxic downstream products such as aminochrome, salsolinols, and 5-S-cysteinyl-dopamine (Cys-DA) (Chen et al. 2008; Hastings et al. 1996; Miyazaki & Asanuma, 2008; Montine et al. 1997; Segura-Aguilar et al. 2014; Stansley & Yamamoto, 2013; Storch et al. 2002). Dopamine can form quinoprotein adducts with α-synuclein (Bisaglia et al. 2010), although in this regard DOPAL is more potent (Jinsmaa et al. 2020).

Based on previous studies, increased activity of TH has the capacity to facilitate the development of oxidative stress via two main processes. First, ROS can be generated during catecholamine synthesis, previously shown in vitro; and second, elevated synthesis may result in increased levels of cytosolic dopamine, which promotes oxidative stress through metabolic and spontaneous oxidation. To evaluate the specific effect of elevated TH in vivo, we developed a novel line of transgenic mice over-expressing functional TH. We hypothesized that an increase in the enzymatic activity of TH would increase oxidative stress and augment endogenous levels of both enzymatic and spontaneous oxidation products of dopamine. TH over-expressing mice have been produced previously (Kaneda et al. 1991); however,

our model is the first to achieve functional over-expression of TH and increased dopamine synthesis that are restricted to endogenous catecholaminergic regions.

2 | MATERIALS AND METHODS

Experiments were conducted in adult mice (male and female), 3–5 months of age (for experimental design, see Figure 1). Mice were housed on a 12-hr light–dark cycle, with food and water provided ad libitum. No randomization was performed to allocate subjects in the study. Mice within a genotype were allocated arbitrarily to the experimental groups such that each group contained comparable numbers of males and females. Group sizes were based on previous work (Masoud et al. 2015; Salahpour et al. 2008). In most cases, the experimenter was not aware of the genotype of the mice until the point of statistical analysis. Western blots were an exception, as these were loaded such that samples within a genotype or treatment group neighboured each other on the blot.

A total of 332 mice were used for this study, inclusive of all experimental groups and genotypes. Effort was made to minimize anxiety and suffering by habituating animals to behavioural suites, and ensuring that mice were accustomed to the experimenters' touch and scent.

Anaesthesia (avertin) was verified by the toe-pinch and eye-brush methods, and by observing a depression in respiratory rate (i.e. that breathing had appreciably slowed). Shortly in advance of experiments requiring anaesthesia, a 20-mL stock volume of avertin was prepared: in a 1.5-mL Eppendorf tube, 0.5 ml of 2-methyl-2-butanol (Sigma, cat. no. 152463) was added to 0.25 g of 2,2,2-tribromoethanol (Sigma, cat. no. T48402). The solution was heated slightly (37–40℃) and mixed well. The solution was added slowly to sterile ddH_2O, and topped to a total volume of 20 ml; the stock solution (1.25 g/ml) was then sterilized through a 0.22-μm filter. Aliquots were stored in the dark at 4℃, and prepared fresh weekly; aliquots were thawed in the dark before use. Mice were injected intraperitoneally at a dose of 200 mg/kg.

Euthanasia was performed with the guidance and approval of the Animal Care Committee. Procedures conformed to the recommendations of the Canadian Council on Animal Care, with protocols reviewed and approved by the University of Toronto Faculty of Medicine and Pharmacy Animal Care Committee (protocol number 20011466).

2.1 | Production of TH-over-expressing mice using BAC transgenesis

Mice over-expressing TH were created by bacterial artificial chromosome (BAC) transgenesis using an artificial chromosome that contains the murine *Th* locus as well as approximately 90 kb of genomic DNA upstream and downstream of the gene (RP23-350E13, Genome Sciences), using previously described methods
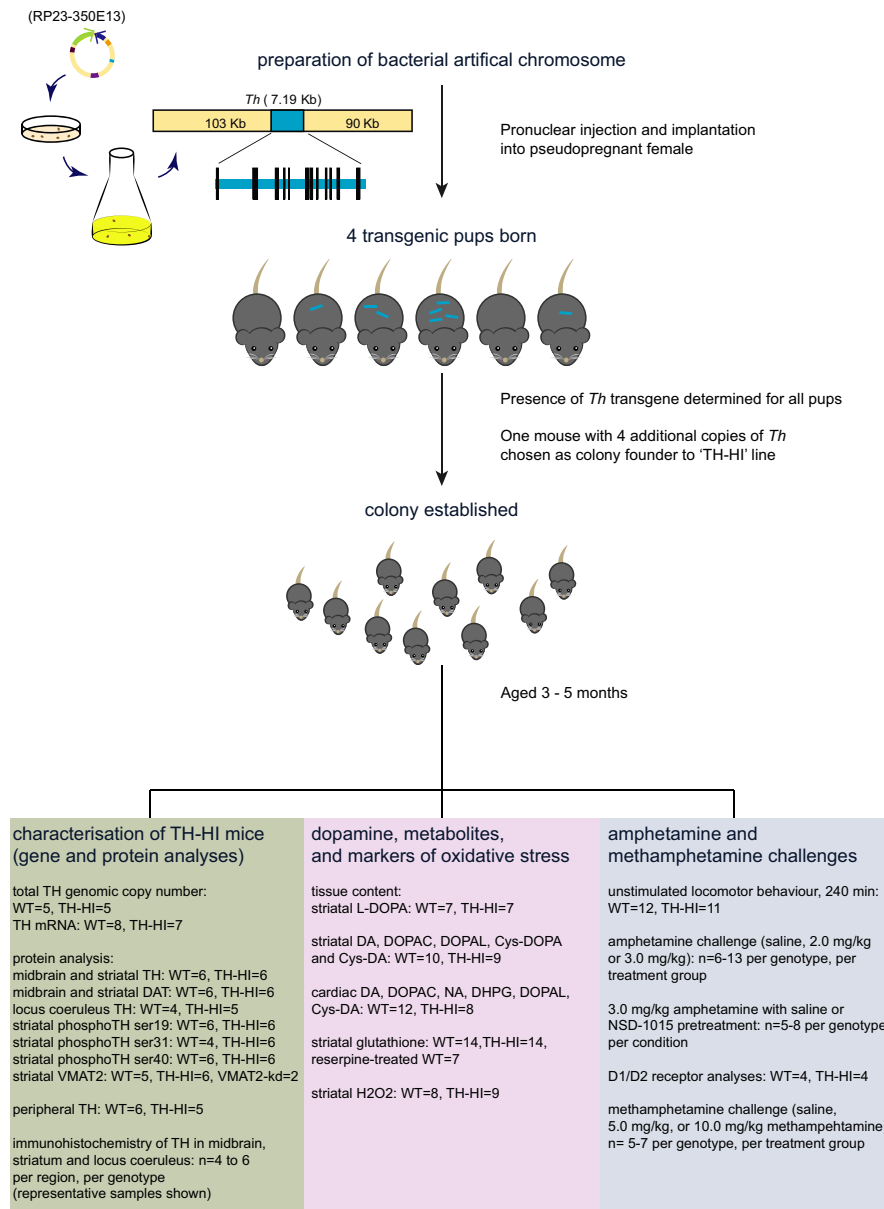
FIGURE 1 Experimental design. A bacterial artificial chromosome (BAC) carrying the tyrosine hydroxylase gene (*Th*, 7.19Kb) as well as 103 Kb and 90 Kb of genomic DNA upstream and downstream of the gene was selected (RP23-350E13). Bacterial colonies were grown on a chloramphenicol-spiked lysogeny broth (LB) agar plate, and single colonies were randomly selected for growth in liquid LB media (12.5 μg/ml chloramphenicol). The colonies were verified by PCR-based genotyping using primers that amplify a sequence overlapping the BAC vector and the *Th* gene. The BAC DNA was isolated and purified using a NucleoBond BAC 100 preparation kit. After resuspension, the DNA preparation was inserted into fertilized oocytes using pronuclear microinjection, then implanted into a pseudopregnant mother. Of the first litter born to her, there were four pups identified as transgenic. A pup that had six total copies of the *Th* gene (i.e. 4 transgenic copies) was used as the founder to a novel line of TH over-expressing mice, 'TH-HI'. From this mouse, a colony was established. Adult mice approximately 3–5 months of age were used for further studies. These experiments fell into three main groups: those that characterized the novel TH-HI mouse line (gene, mRNA and protein analyses); those that analysed tissue content of dopamine, its metabolites, and markers of oxidative stress; and those that assessed the locomotor response to compounds known to affect the dopaminergic system, amphetamine, and methamphetamine. The number of mice (n) used for each experiment is indicated. Cys-DOPA, 5-S-cysteinyldopa; Cys-DA, 5-S-cysteinyldopamine; D1/D2, dopamine receptors type 1 and 2; DA, dopamine; DHPG, 3,4-dihydroxyphenylethylene glycol; DAT, dopamine transporter; DOPAC, 3,4-dihydroxyphenylacetic acid; DOPAL, 3,4-dihydroxyphenylacetaldehyde; L-DOPA, l-3,4-dihydroxyphenylalanine; n, number of mice; NA, noradrenaline; TH, tyrosine hydroxylase; TH-HI, transgenic mice over-expressing tyrosine hydroxylase; VMAT2, vesicular monoamine transporter 2; VMAT-kd, VMAT2-knockdown mice; WT, wild-type mice

(Lohr et al. 2014; Salahpour et al. 2008). Because BACs often contain the endogenous promotor for a gene of interest, gene expression is restricted to regions that endogenously express it. Bacterial colonies were grown on a chloramphenicol-spiked lysogeny broth (LB) agar plate, and single colonies were randomly selected for growth in liquid LB media (12.5 μg/ml chloramphenicol). The colonies were

verified by PCR-based genotyping using primers that amplify a sequence overlapping the BAC vector and the *Th* gene (forward, *5'-gaaggctctcaagggcatc*; reverse, *5′-acaggtcaggctctcaggtc*).

The BAC DNA was isolated using a NucleoBond BAC 100 preparation kit (Macherey-Nagel, cat no. 740579) and resuspended in injection buffer (spermine, 0.03 mM; spermidine, 0.07 mM). Pronuclear microinjections were performed at the Emory University Transgenic Facility. Transgenic positive pups were identified by PCR-based genotyping (*5'-aggagctgactgggttgaag*; reverse, *5′-tcgtggcctgttgtgagtag*); again, primer sequences overlapped the vector and gene sequences, thereby differentiating transgenic *Th* from native *Th*. Of the F1 generation, a mouse determined by qPCR to possess 6 total copies of genomic *Th* was used as a founder for a transgenic high copy line, "TH-HI." Transgenic mice were maintained on a C57Bl/6J background.

2.2 | Determination of gene copy number and total *Th* mRNA levels

2.2.1 | Gene copy number

Genomic DNA was isolated from tail biopsy following Proteinase K digestion and isopropanol precipitation (Ballester et al. 2004; Burkhart et al. 2002), and cleaned using a chloroform-ammonium acetate wash method. Quantitative PCR (qPCR) was used to determine total allelic copy number of *Th*, inclusive of both native alleles and transgenic copies (Ballester et al. 2004; Shepherd et al. 2009). Amplicons of the *Th* genomic sequence were generated using designed primers (forward: *5'-caccagtcctgagtttcctatt*, reverse: *5'-ctggatcacactccaccatatc*) and measured relative to those of a common reference gene that encodes the transferrin receptor (*Tfrc*; forward: *5'-cagtcatcagggttgcctaata*, reverse: *5'-atcacaacctcaccatgtaact*). Relative quantification of *Th* and *Tfrc* were obtained using the GoTaq® qPCR Master Mix (Promega, cat no. A6002) on the Applied Biosystems 7500 Real-Time PCR System. The PCR protocol used for all reactions was as follows: 2 min at 50℃, 10 min at 95℃, 40 repeats of 95℃ for 15 s, and 1 min at 60℃. Analysis of gene copy number was based upon the 2-ΔΔCT method as previously described (Livak & Schmittgen, 2001; Pfaffl, 2001; Schmittgen & Livak, 2008).

2.2.2 | mRNA

Reverse-transcriptase qPCR was also used to determine total levels of mRNA on midbrain regions dissected from a 1-mm coronal section of brain, which was previously removed and frozen in 2-methybutane over dry ice and stored at −80℃ (Hu et al. 2009); 300 ng of RNA was used to obtain complementary DNA using SuperScript III Reverse Transcriptase (Invitrogen, cat no. 11752-250) according to the manufacturer's instructions. As before, quantification of mRNA levels was obtained using the GoTaq® qPCR Master Mix on the Applied Biosystems 7500 Real-Time PCR System. To ensure that the level of *Th* mRNA was normalized to the volume of dopaminergic

cells within the dissected area, *Th* mRNA levels (forward primer: *5'-cgggcttctctgaccaggcg*; reverse primer: *5'-tggggaattggctcaccctgct*) were presented as a ratio of the dopamine transporter (DAT), *Slc6a3*, mRNA levels (forward primer: *5'-ggcctgggcctcaacgacac*; reverse primer: *5'-ggtgcagcacaccacgtccaa*). Phosphoglycerate kinase 1 (*Pgk1*; forward primer:*5'-ggcctttcgacctcacggtgt*; reverse primer: *5'-gtccaccctcatcacgacccg*) was used as the reference gene, and relative quantification of both targets was obtained using the 2-ΔΔCT method.

2.3 | Western blotting

2.3.1 | Total TH and DAT in the central and peripheral systems

Western blots were performed to quantify TH and DAT protein expression in the dopaminergic nigrostriatal pathway, using the sodium-potassium pump (Na$^+$/K$^+$-ATPase) as a loading control. The midbrain (substantia nigra) and striatum were dissected from freshly harvested brains, flash-frozen, and mechanically homogenized in RIPA buffer [50 mM Tris·HCl, pH 7.4; 150 mM NaCl; 1% Nonidet P-40; 0.5% sodium deoxycholate; 0.1% sodium dodecyl sulphate (SDS)] with protease inhibitors (pepstatin A, 5 μg/mL; leupeptin, 10 μg/mL; aprotinin, 1.5 μg/mL; benzamidine, 0.1 μg/mL; PMSF, 0.1 mM). Samples were centrifuged at 21,130 g for 15 min to remove cellular debris and the supernatant was collected. Protein concentrations were determined using a Pierce bicinchoninic acid (BCA) assay (Thermo Scientific, cat no. 23225). Samples were prepared to the desired loading amount (striatum, 25 μg; midbrain, 60 μg) in a solution containing 1× SDS sample buffer (4× solution: 3.4 g Tris Base, 8.0 g SDS, 40 ml glycerol in 1 L dH$_2$O, pH 6.8), 0.05% β-mercaptoethanol (BME), and RIPA buffer. Preparations were heated to 55℃ for 10 min, separated by 10% SDS/PAGE, and wet-transferred to polyvinylidene difluoride (PVDF) membranes (FluoroTrans, Pall, cat no. CA29301-856). Membranes were blocked in Li-COR buffer for 60 min at room temperature and incubated overnight at 4℃ with rat anti-DAT (1:750; Millipore, cat no. MAB369, RRID: AB_2190413) and rabbit anti-Na$^+$/K$^+$-ATPase (1:2000; cat no. 3010, RRID: AB_2060983) in the same buffer. After washing, protein bands were revealed by incubating with the fluorescence-labelled secondary antibodies donkey anti-rat IRdye 800CW (1:5,000; Rockland, cat no. 612-732-120, RRID:AB_220173) and goat anti-rabbit AlexaFluor AF680 (1:5,000; Invitrogen, cat no. A21076, RRID: AB_2535736) for 60 min at room temperature. Without stripping, membranes were then blocked a second time in 5% non-fat milk and probed with rabbit anti-TH (1:3,000; Millipore, cat no. AB152, RRID: AB_390204) overnight at 4℃, which was again revealed with goat anti-rabbit AlexaFluor AF680.

Using similar methods, TH protein levels in both central and peripheral noradrenergic regions were examined. Tissue from the TH-rich locus coeruleus and the adrenal medulla was extracted, prepared, and run as described above (loading 60 μg per sample for the locus coeruleus, 20 μg per sample for the adrenal medulla). PVDF

membranes were probed for rabbit anti-TH as described above. Mouse anti-β-tubulin (1:1,000; Developmental Studies Hybridoma Bank, E7) and mouse anti-GAPDH (1:3,000; Sigma, cat no. G8795, RRID:AB_1078991) were used as loading controls for the locus coeruleus and adrenal medulla (respectively), and revealed with donkey anti-mouse IRdye 800CW (1:5,000; Rockland, cat no. 610-731-002, RRID: AB_1660943).

2.3.2 | Phosphorylated TH

Levels of TH phosphorylated at serine residues 19, 31, and 40 were also measured, as a representation of TH in an active conformation. In a separate set of experiments, striatal samples were quickly dissected, flash-frozen, and homogenized in RIPA containing phosphatase inhibitors (sodium pyrophosphate, 2.5 mM; β-glycerophosphate, 1.0 mM; sodium fluoride, 50 mM; sodium orthovanadate, 1.0 mM), in addition to the protease inhibitors listed above. As before, striatal samples were prepared to the desired loading amount of 25 µg, run on a 10% SDS/PAGE gel, and transferred to PVDF membrane. Membranes were incubated overnight at 4℃ in solutions containing rabbit anti-phosphoTH-Ser19 (1:2000; PhosphoSolutions, cat no. p1580-19), rabbit anti-phosphoTH-Ser31 (1:1,000; PhosphoSolutions, cat no. p1580-31), or rabbit anti-phosphoTH-Ser40 (1:2000; PhosphoSolutions, cat no. p1580-40). Proteins were revealed using goat anti-rabbit AF680 (1:5,000) before being stripped, and reprobed using mouse anti-TH (1:2,500; Sigma, cat no. T2928, RRID:AB_477569) and mouse anti-GAPDH in 5% non-fat milk. These were revealed with donkey anti-mouse IRdye 800CW.

2.3.3 | VMAT2

Levels of VMAT2 were assessed using pre-cast gels and MOPS (3-(N-morpholino)propanesulfonic acid) buffers, with rabbit anti-VMAT2 antibody (1:10,000, in-house antibody), as previously described (Cliburn et al. 2017; Lohr et al. 2014). The VMAT2 protein was revealed with goat anti-rabbit 800 (1:5,000; Rockland, cat no. 611-131-002, RRID: AB_1660973) by incubating for 60 min at room temperature, and membranes were reprobed for TH and GAPDH as above.

For all of the above westerns, proteins were visualized using the LiCOR Odyssey system. Densitometric analyses were conducted using Image Processing and Analysis in Java (ImageJ) software (http://rsb.info.nih.gov/ij/index.html). For full (uncropped) blots, see https://osf.io/9q7b5/?view_only=c580d782a77d475984bb35eb41738279.

2.4 | Radioligand binding

Radioligand binding was used to assess D1 and D2 dopamine receptor levels in the striatum as previously described (Ghisi et al. 2009).

Striatal tissues were rapidly dissected and homogenized in lysis buffer (50 mM Tris–HCl, pH 7.4; 120 mM NaCl; 1 mM EDTA) containing protease inhibitors. The homogenate was centrifuged at 1,000 g for 10 min (4℃) to remove cellular debris and nuclei, after which supernatant was centrifuged at 40,000 g for 20 min (4℃); the pellet was then resuspended in lysis buffer and centrifuged again under the same conditions. The final pellet was resuspended in assay buffer (50 mM Tris–HCl (pH 7.4), 120 mM NaCl, 5 mM KCl, 2 mM CaCl2, and 1 mM MgCl2). Protein concentration of membranes was determined using BCA protein assay.

For D1 receptor saturation experiments, 50 µl of prepared striatal membranes (1.2 µg/µl) was incubated with 50 µl of 16 nM [3H]-SCH23390, a D1 receptor antagonist, as well as 50 µl of 100 mM ketanserin, a serotonin receptor antagonist, to prevent radioligand binding to these receptors. The reaction was performed in 200 µl of assay buffer for 1 hour, at room temperature. In parallel reactions, nonspecific binding was measured using non-radiolabelled flupenthixol (10 µM), a D1/D2 receptor antagonist. For D2 receptor saturation experiments, 150 µl of prepared striatal membranes (0.5 µg/µl) was incubated with 50 µl of [3H]-spiperone (3 nM), a D2 receptor antagonist. This reaction was performed in 250 µl of assay buffer for 2 hours at room temperature; non-specific binding was measured in parallel using non-radiolabelled haloperidol (6 µM), a D2 antagonist.

All reactions were terminated by filtration over Brandel GF/C glass fibre filters and washing with cold assay buffer. Filters were incubated overnight in high flash point scintillation cocktail (5 ml, Lefko-Fluor). Radioactivity was counted using a liquid scintillation counter. Counts of non-specific binding were subtracted from total binding to obtain specific [3H]-SCH23390 or [3H]-spiperone binding, which corresponds to D1 or D2 binding, respectively, and converted to fmol/mg tissue for final results. The experimenter was blinded until the point of statistical analyses.

2.5 | Immunohistochemistry

Adult mice were anaesthetized with avertin (200 mg/kg) prior to perfusions, and intracardially perfused with phosphate-buffered saline (PBS) at a flow rate of 80 ml/h for 2 min, followed by 4% paraformaldehyde in PBS for approximately 10 min. The brains were removed and stored in 4% paraformaldehyde in PBS overnight at 4℃, then transferred to a 30% sucrose solution for cryoprotection for 48 hr at 4℃. Tissues were blocked in freezing media HistoPrep (Fisher Chemical, cat no. SH75-125D) and cut into 40 µm coronal sections using a cryostat (Leica, CM1510). Midbrain and striatum sections were immunostained for TH and DAT, using methods previously described (Vecchio et al. 2014); TH and the noradrenaline transporter (NET) were immunostained in the locus coeruleus. *Primary antibodies*: rabbit anti-TH (1:2000), rat anti-DAT (1:200), and anti-NET (1:500; MAb Technologies, cat no. NET05-2, RRID:AB_2571639). *Secondary antibodies*: anti-rabbit AF680 (1:4,000), anti-rat IRdye 800 (1:2000), and anti-mouse IRdye 800CW (1:2000). Slides were scanned using the LiCOR Odyssey

system, with a focus offset of 0.90–1.0 mm. For original scan images, see https://osf.io/2tqwe/?view_only=c9d0d187221c4ca989bc93455534b98d.

2.6 | Tissue catechol contents

Catecholamines (dopamine, noradrenaline), their respective metabolites (DOPAC, DHPG), and cysteinylated catechols were measured in the striatum and in heart tissue, using methods previously described (Casida et al. 2014; Goldstein et al. 2013; Wey et al. 2012). Briefly, striata were dissected and flash frozen in liquid nitrogen. Frozen tissue samples were homogenized in a mixture of 20:80 of 0.2 M phosphoric acid: 0.2 M acetic acid. The supernate was assayed by batch alumina extraction followed by high-performance liquid chromatography (HPLC) with electrochemical detection, using a Spheri-5 RP-18, 5 μm, 30×2.6 mm guard column (PerkinElmer, Part No. 07110013) and C18, 5 μm, 120 Å, 4.6×250 mm analytic column (Thomson Instruments, Part No. BA400-046250), on a Waters Model 710B (WISP) automated sample processor (Waters Associates). The mobile phase consisted of 13.8 g monobasic sodium phosphate, 28–40 mg octanesulfonic acid, 50 mg EDTA, and 0–5 ml acetonitrile in 1 L of HPLC-grade water, with pH adjusted to 3.2–3.3 using 85% phosphoric acid.

In a separate set of experiments, a single IP injection of the AADC inhibitor NSD-1015 (100 mg/kg) was administered to prevent the rapid conversation of L-3,4-dihydroxyphenylalanine (L-DOPA) to dopamine (Jones, Gainetdinov, Jaber, et al., 1998). Mice were sacrificed by cervical dislocation 40 min following the injection, at which time the striata were dissected and flash frozen in liquid nitrogen. Unilateral striata were weighed and homogenized in 40 μL per mg sample of 0.1 M perchloric acid ($HClO_4$) spiked with both 2,3-dihydroxybenzoic acid (DHBA, an internal standard) and 100 ng/ml sodium metabisulphite (Caudle et al. 2007; Moron et al. 2000), and then centrifuged 10,000 g for 10 min at 4℃. The supernatant was carefully removed and filtered through a 0.22-μm membrane (Ultrafree-MC GVWP filters; Millipore, cat no. UFC30GV00) by centrifugation at 10,000 g for 2 min at 4℃. Tissue content analyses were conducted using an $AgAgCl^-$ electrochemical detector (LC-4C Amperometric Detector; BASi) set at an oxidizing potential of + 0.75 V, and a Hypersil Gold C18 column (150×3 mm, particle size of 5 μm; Thermo Fisher Scientific). The mobile phase was composed of 5.99 g monobasic sodium phosphate, 200 μM EDTA, 0.684 g sodium chloride, 60 mg octyl sodium sulphate, and 95 ml of methanol in 1 L HPLC-grade water (pH 2.43). Analytes were quantified against standard curves (Sigma, cat no. D9628) (all chemical standards from Sigma, purity >98%). The experimenter was blinded until the point of statistical analyses.

2.7 | Glutathione assay

Glutathione concentrations in the striatum were measured using a glutathione assay kit (Cayman, cat no. 703002), and determined using the kinetic method. Brains were removed and quickly rinsed in ice-cold PBS to remove blood on the exterior of the brain; striatal

and cortical samples were then dissected and flash frozen in liquid nitrogen. The weight of the frozen tissue was taken, and the tissue was homogenized in ice-cold MES buffer (0.4 M 2[N-morpholino] ethanesulphonic acid, containing 1 mM EDTA; pH 6–7; 10 μL per mg of tissue). Homogenate was spun at 10,000 g for 15 min at 4℃. The supernatant was transferred to a clean tube, and deproteinated using metaphosphoric acid (MPA) and 4 M triethanolamine (TEAM) solution, as per kit instructions. A subgroup of wild-type mice were injected with 5 mg/kg of reserpine (injection volume: 0.2 ml/g) 120 min prior to dissection, as a positive control of oxidative stress (Spina & Cohen, 1989). Reserpine is known to irreversibly block VMAT2, leading the accumulation of cytosolic dopamine (Bernstein et al. 2014; de Freitas et al. 2016). In turn, this can lead to increased metabolism, and enzymatic and spontaneous oxidation, and has been shown to induce oxidative stress and reduce glutathione in dopaminergic cells (Spina & Cohen, 1989). Cortical tissue was used as a negative control.

2.8 | H_2O_2 assay

H_2O_2 concentrations in striatal samples were measured as per kit instructions (Abcam, cat no. ab102500), using the colorimetric method. Briefly, striata were dissected, homogenized in ice-cold buffer, and spun for 5 min at top speed (4℃). Supernatant was immediately deproteinated using perchloric acid (PCA, 4 M) and potassium hydroxide (KOH, 2 M) and samples were spun (15 min, 13,000 g, 4℃), after which supernatant was stored at −80℃ until use. In preparation for the assay, samples were diluted in assay buffer 1:10, with 50 μl of diluted sample added to 50 μl of reaction mix. Plates were read at OD570 nm. The experimenter was blinded until the point of statistical analyses.

2.9 | Locomotor activity and amphetamine challenge

Experiments began at approximately 8:00 a.m., with mice introduced to the experimental room half an hour prior to beginning.

Locomotor activity was measured in automated locomotor activity monitors (Accuscan Instruments). Baseline gross locomotor activity was measured for 4 hr, with total distance travelled recorded in 5-min bins (or epochs). In amphetamine-challenge experiments, output parameters of total distance travelled and stereotypic behaviours were collected in 5-min bins over the course of the test period. Mice were placed in the activity monitor chamber (20 cm ×20 cm) and measured under baseline conditions for 60 min. Following baseline recording, mice received an injection of saline or 2 mg/kg or 3 mg/kg amphetamine (dissolved in 0.9% wv^{-1} saline) and were observed for an additional 90 min. All injections were intraperitoneal (IP) at an injection volume of 0.1 ml/g (Salahpour et al. 2008; Vecchio et al. 2014).

We sought to confirm that augmented amphetamine responses in TH-HI mice result from increased de novo dopamine synthesis. Wild-type and TH-HI mice were separated into two groups each. Sixty minutes prior to administration of amphetamine (3.0 mg/kg),

one group received a control injection of saline and the other, an IP injection of NSD-1015 (100 mg/kg), blocking the synthesis of de novo dopamine. As before, mice were allowed to habituate during this time. Locomotor activity was recorded for an additional 90 min following the injection of amphetamine. Due to the potential stress of the first injection combined with the introduction to the recording chambers, the first 15 min following the first injection were excluded from analyses of the baseline (pre-amphetamine) period. The experimenter was blinded until the point of statistical analyses.

2.10 | Methamphetamine challenge

Adult wild-type and TH-HI mice were randomly assigned to treatment groups that would receive 4 injections of 0.9% saline, 5.0 mg/kg or 10 mg/kg of (+)-Methamphetamine HCl (Sigma; dissolved in 0.9% saline). Treatments were administered through a subcutaneous injection as previously described (Lohr et al. 2015). The first dose was administered 60 min after baseline core body temperature was measured using a rectal thermometer. Three additional equivalent doses followed, administered at 2-hr intervals (i.e. 180, 300, and 420 min following the initial injection). Core body temperature was measured at the time of each injection. Mice were killed by rapid decapitation 48 hr following the first injection, and the striatum was dissected and flash-frozen in liquid nitrogen for protein analyses by Western blot, using standard methods described above. The experimenter was blinded until the point of statistical analyses.

2.11 | Statistical analyses

All statistical analyses were performed for each group by Student's *t*-test, one-way ANOVA, or two-way ANOVA. Post hoc analyses were performed using the Bonferroni test, Tukey's test (all pairwise comparisons), or the Dunnett's test, as appropriate. The *F*-test was used to verify equal variance. Where there was unequal variance between two groups analysed by *t*-test, a Welch's correction was performed. The Shapiro–Wilk test was used to assess normality of all data. Where this test revealed that distribution was not normal, *t*-tests were replaced with non-parametric Mann–Whitney tests. The Grubbs test was used to identify statistical outliers, which were excluded if found. Significance is reported where $p < .05$. No sample calculations were performed prior to testing, but sample sizes were based on previous studies. All statistical testing was carried out using GraphPad Prism version 9.

3 | RESULTS

3.1 | Production of TH-over-expressing (TH-HI) mice

Purified BAC DNA containing the murine *Th* gene was microinjected into the pronucleus of donor oocytes, which were then implanted

into pseudo-pregnant females yielding 4 transgenic pups. The total copy number of the *Th* gene was determined for all pups born to the host mothers using quantitative PCR. A pup carrying 6 total copies of the *Th* gene—2 endogenous alleles and 4 additional copies of *Th* that resulted from integration of the transgene—was assigned as the founder of the TH-HI line ($p \leq .0001$, *t*-test) (Figure 2a). Commensurate with a 3-fold increase in gene copy number, *Th* mRNA levels in the midbrain of TH-HI mice were 3 times higher than that of wild-type littermates (measured relative to a commonly used reference gene, *Pgk1*; $p \leq .0001$, *t*-test) (Figure 2b).

Transgenic mice did not differ in size or appearance relative to sex- and age-matched wild-type littermates, nor did they have apparent differences in general health. Mice did not have difficulties breeding or delivering pups, and had an average litter size of 5.2 pups (breeding pairs were retired at 8–12 months of age).

3.2 | TH protein expression is increased in central and peripheral sites of catecholamine production in TH-HI mice

TH-HI mice showed a 3-fold increase in the optical density of TH protein in the midbrain ($p = .0003$, *t*-test) (Figure 2c, d) and striatum ($p \leq .0001$, *t*-test) (Figure 2f, g), revealing that the amount of total protein translated is proportional to the observed increase in gene copy number and mRNA. There was no change in the level of DAT protein between wild-type and TH-HI mice (midbrain: Figure 2e, $p = .32$, *t*-test; striatum: Figure 2h, $p = .80$, *t*-test).

Immunostaining revealed that TH protein was expressed in similar patterns in the midbrain and striatum of wild-type and transgenic mice (Figure 2j, i). No evidence of ectopic expression of TH was detected in the regions that surround the striatum in the forebrain, or the substantia nigra and ventral tegmental area in the mesencephalon.

To assess protein expression in the noradrenergic system, we quantified total TH protein in the locus coeruleus. There was an approximate 3-fold increase in TH optical density, comparable to the increase in TH observed in dopaminergic regions ($p = .0014$, *t*-test) (Figure S1a, b).

Immunostaining showed that TH expression patterns in the locus coeruleus of transgenic mice mirrored that of wild-type littermates, again without evidence of ectopic expression (Figure S1c).

Peripheral expression of TH was measured in the adrenal medulla, where it is highly concentrated (de Diego et al. 2008). In transgenic mice, total TH protein in the adrenal medulla was approximately 2.5 times higher than that of wild-type littermates ($p = .0035$, *t*-test) (Figure S1d, e), demonstrating successful overproduction of TH in both peripheral and central nervous systems.

3.3 | TH-HI mice have increased levels of phosphorylated TH and TH enzymatic activity

Western blot analyses showed an approximate 3-fold increase in the optical density of striatal TH phosphorylated at Ser40, Ser31, and
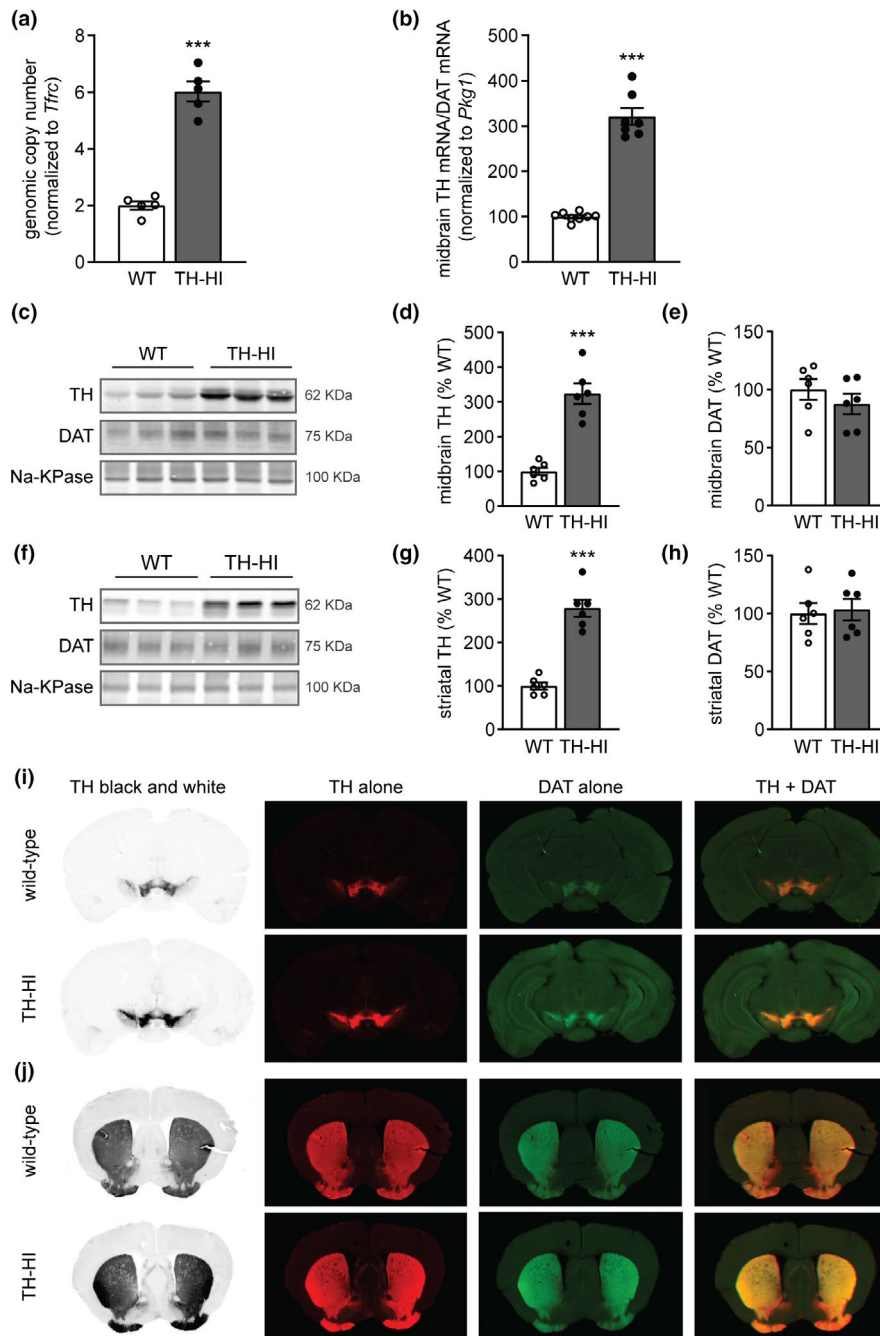
FIGURE 2 Tyrosine hydroxylase over-expressing mice. (a) Genomic copy number of tyrosine hydroxylase (TH) in TH-HI mice relative to wild-type (WT) littermates. Copy number is determined by comparison of the cycle threshold to that of the reference gene, *Tfrc*. ($n = 5$ per group; $p \leq .0001$, *t*-test). (b) *Th* mRNA levels in TH-HI and WT mice, relative to the reference gene *Pkg1*. All values are normalized to dopamine transporter (DAT) mRNA levels in the same sample, which is used as a marker of dopaminergic cells, and shown relative to wild-type levels (WT $n = 8$, TH-HI $n = 7$; $p \leq .0001$, *t*-test with Welch's correction). (c) Midbrain TH and DAT protein expression is shown in adult mice by western blot together with the loading control, Na-KPase (representative samples) ($n = 6$ per group). (d) Average optical density of midbrain TH protein in TH-HI mice (normalized to Na-KPase), shown relative to wild-type mice ($p = .0003$, *t*-test with Welch's correction). (e) Average optical density of midbrain DAT protein in TH-HI mice (normalized to Na-KPase), shown relative to wild-type mice ($p = .34$, *t*-test). (f) Striatal TH and DAT protein expression is shown in adult mice by western blot together with the loading control, Na-KPase (representative samples) ($n = 6$ per group). (g) Average optical density of striatal TH protein in TH-HI mice (normalized to Na-KPase), shown relative to wild-type mice ($p \leq .0001$, *t*-test). (h) Average optical density of striatal DAT protein in TH-HI mice (normalized to Na-KPase), shown relative to wild-type mice ($p = .80$, *t*-test). (i) Immunohistochemistry reveals protein expression patterns of TH (red) and DAT (green) in the midbrain. Yellow represents co-localized TH and DAT. (j) Protein expression patterns of TH (red) and DAT (green) in the striatum. Yellow represents co-localized TH and DAT. n = number of mice. ($p < .001$, ***) Mean $\pm$ *SEM*

Ser19, demonstrating that the level of phosphorylated TH increases in proportion to total TH protein levels in transgenic mice (Ser40, $p \le .0001$, t-test; Fig. S2a, b) (Ser31, $p \le .0001$, t-test; Figure S2d, e) (Ser19, $p \le .0001$, t-test; Figure 2g, h). The proportion of TH that was phosphorylated relative to the total pool did not significantly differ between wild-type and TH-HI mice at any residue (Figure S2c, f, i).

Elevated levels of phosphorylated TH in TH-HI mice indicate that the over-expressed enzyme is in an active state, and in a conformation less susceptible to feedback inhibition by catechols (Daubner et al. 2011). In turn, the extent of L-DOPA accumulation in striatal samples provides a measure of TH enzymatic activity in vivo (Ferris et al. 2014). Therefore, we next assessed striatal levels of L-DOPA, the direct product of TH. In TH-HI mice, L-DOPA accumulation following injections of NSD-1015, which blocks aromatic L-amino acid decarboxylase (AADC), was twice that in wild-type animals ($p \le .0001$, t-test) (Figure 3a). The increase in L-DOPA accumulation directly shows that the over-expressed TH protein is functional, increasing the rate of dopamine synthesis 2-fold in TH-HI mice.

3.4 | Striatal dopamine levels and tissue dopamine turnover are increased in TH-HI mice

There was a significant effect of genotype on striatal tissue content of dopamine, which rose over wild-type levels by
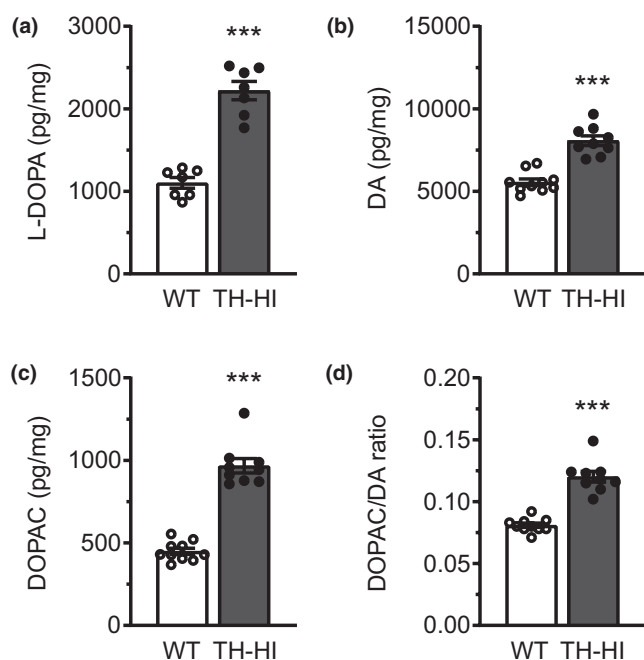
FIGURE 3 Synthesis and tissue content of dopamine and its metabolites in the striatum of adult mice. TH-HI mice show elevated tissue content of (a) L-DOPA accumulation following NSD-1015 injections (WT $n = 7$, TH-HI $n = 7$; $p \le .0001$, t-test), (b) dopamine (DA) (WT $n = 10$, TH-HI $n = 9$; $p \le .0001$, t-test), (c) 3,4-dihydroxyphenylacetic acid (DOPAC) (WT $n = 10$, TH-HI $n = 9$; $p \le .0001$, Mann–Whitney test), and (d) DOPAC to DA ratio (WT $n = 10$, TH-HI $n = 9$; $p \le .0001$, Mann–Whitney test). $n =$ number of mice. ($p \le .001$, ***) Mean $\pm$ *SEM*

approximately 50% ($p \le .0001$, t-test) (Figure 3b). The total tissue content of DOPAC was also elevated by more than 2-fold in the TH-HI mice ($p \le .0001$, Mann–Whitney test) (Figure 3c). In addition, DOPAC/dopamine ratios were increased in TH-HI mice ($p \le .0001$, Mann–Whitney test) (Figure 3d), representative of increased dopamine turnover.

3.5 | VMAT2 levels are unchanged in TH-HI transgenic mice

We next sought to determine if the expression of VMAT2 was upregulated in TH-HI mice to accommodate the increased dopamine production. There was no difference in VMAT2 protein levels between TH-HI mice and wild-type littermates (Figure S3).

3.6 | Oxidative stress is enhanced in TH-HI mice

An elevated presence of DOPAC can suggest accelerated ROS production, as H_2O_2 is produced by MAO during the first steps of dopamine metabolism; in addition, increased levels of DOPAC could be accompanied by an elevated presence of reactive intermediates such as DOPAL, as well as increased reactive species as a result of metabolic oxidation. Concomitant with increased dopamine production and increased dopamine turnover, H_2O_2 was found to be elevated in the striatum of TH-HI mice by approximately 30% ($p = .031$, t-test) (Figure 4a). In addition, levels of glutathione—which acts to neutralize H_2O_2—were significantly reduced in the striatum of adult TH-HI mice ($p = .0019$, one-way ANOVA), but not in cortical tissue (Figure 4b, c).

Wild-type mice were treated with reserpine (5 mg/kg) as a positive control. Reserpine acts by irreversibly blocking VMAT2, in turn inhibiting the transport of catecholamines from the cytosol to the vesicles, leading to oxidative stress and reduced glutathione levels (de Freitas et al. 2016; Spina & Cohen, 1989). As expected, reserpine treatment of WT animals results in reduced glutathione levels (Figure 4b). Importantly, the extent of decrease in glutathione levels of reserpine treated WT animals was similar to the basal levels detected in TH-HI (Figure 4b), which is consistent with an elevated presence of ROS in regions where increased TH activity is observed.

3.7 | TH-HI mice have elevated striatal levels of enzymatic and spontaneous oxidation products

TH-HI mice had elevated striatal levels of the reactive intermediate metabolite DOPAL compared with wild-type mice ($p = .010$, t-test) (Figure 4d), resulting from increased enzymatic oxidation. Cysteinyl-L-DOPA and cysteinyl-dopamine were also elevated in TH-HI animals compared with wild-type littermates ($p = .0003$ and $p = .0002$, respectively, t-test) (Figure 4e, f). As an increased presence of
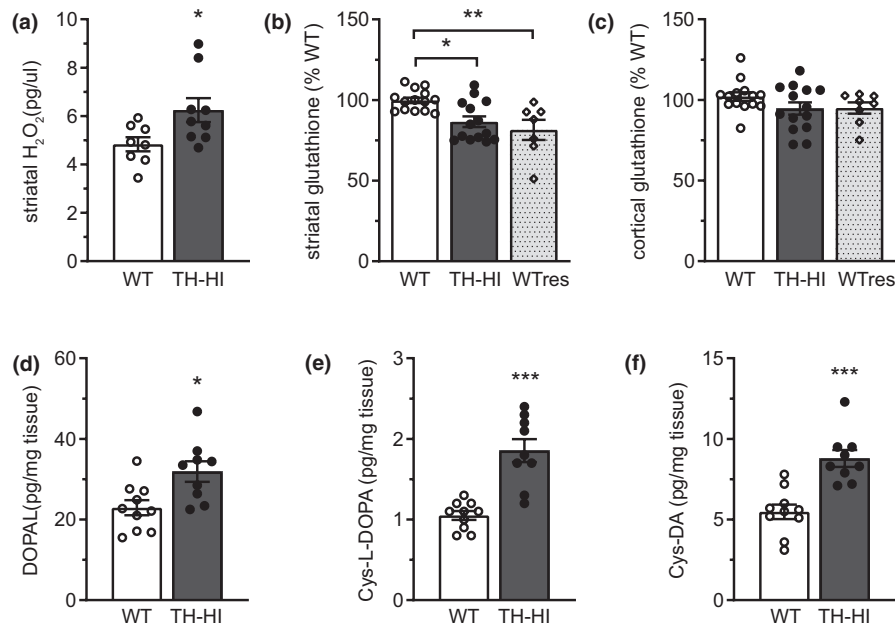
FIGURE 4 Markers of oxidative stress in adult TH-HI mice. (a) Concentration of hydrogen peroxide was found to be elevated in striatal tissue of adult transgenic mice (TH-HI) as compared with wild-type (WT) littermates (WT $n = 8$, TH-HI $n = 9$)($p = .031$, t-test). (b) Total glutathione levels (GSH) were reduced in striatal tissue of TH-HI mice compared with WT mice. No significant difference in striatal GSH levels was detected between transgenic mice and WT mice that had been treated with reserpine 120 min prior to dissections (WTres). (WT $n = 14$; TH-HI $n = 14$; WTres $n = 7$) (all data normalized to WT) ($F_{2, 32} = 7.709$, $p = .0019$, one-way ANOVA, Bonferroni post hoc). (c) No change in GSH levels was detected in cortical samples. (WT $n = 14$; TH-HI $n = 14$; WTres $n = 7$) (all data normalized to WT) ($F_{2, 33} = 1.647$, $p = .21$, one-way ANOVA, Bonferroni post hoc). (d) 3,4-dihydroxyphenylacetaldehyde (DOPAL) levels in the striatum of TH-HI mice were elevated over wild-type levels (WT $n = 10$, TH-HI $n = 9$)($p = .010$, t-test), as were (e) Cysteinylated L-3,4-dihydroxyphenylalanine (Cys-DOPA) levels (WT $n = 10$, TH-HI $n = 9$) ($p = .0003$, t-test with Welch's correction) and (f) Cysteinylated dopamine (Cys-DA) levels (WT $n = 10$, TH-HI $n = 9$) ($p = .0002$, t-test). $n = $ number of mice. ($p \le .05$, *; $p \le .01$, **; $p \le .001$, ***) Mean ± SEM

cysteinylated dopamine is considered an indication of accelerated dopamine auto-oxidation (Chen et al. 2008; Li & Dryhurst, 2001), these findings demonstrate that increased activity of TH alone is sufficient to elevate markers of oxidative stress arising from enzymatic and spontaneous oxidation.

3.8 | TH-HI mice have increased cardiac levels of dopamine and its oxidation products

Past studies have suggested that catecholamine dysfunction and denervation of the heart may occur early in the pathology of Parkinson's disease, preceding the onset of recognizable motor symptoms (Goldstein et al. 2007). To examine whether markers of oxidative stress exist in peripheral tissue, we examined catecholamine content, catecholamine turnover, and cysteinylated catechols in heart tissue. TH-HI mice had increased cardiac concentrations of dopamine ($p \le .0001$, Mann–Whitney test) and DOPAC ($p = .0002$, Mann–Whitney test). There was a trend towards increased dopamine turnover ($p = .054$, t-test) (Figure S4a–c). In addition, there was a significant increase in Cys-DA ($p = .0042$, Mann–Whitney test) (Figure 3g). There were no group differences in levels of noradrenaline or its metabolite DHPG (Figure S4d–f). DOPAL was not detected in any samples of heart tissue.

3.9 | TH-HI mice have potentiated responses to amphetamine

The locomotor behaviour of transgenic mice was not found to differ from their wild-type littermates when measured for up to 4 hr under normal (unstimulated) conditions (Figure 5a); similar results were found during baseline recordings prior to an amphetamine challenge (see minutes 0–60, Figure 5b).

As a functional read-out of enhanced dopamine production and storage, we challenged mice with two doses of amphetamine (2.0 mg/kg and 3.0 mg/kg). Amphetamine treatment results in massive efflux of monoamines through their membrane transporters due to a reversal in the concentration gradient (Heal et al. 2013; Jones et al. 1998; Salahpour et al. 2008; Sulzer et al. 1995). Because of its potent effect on the dopaminergic system, amphetamine is often used to test the integrity of the nigrostriatal pathway, using locomotor activity as an outcome measure (Giros et al. 1996). When challenged with these two doses of amphetamine (2.0 mg/kg and 3.0 mg/kg), TH-HI mice had a greatly potentiated locomotor response to amphetamine, more than doubling total distance travelled in the 90 min (Figure 5b, c). In addition, TH-HI mice showed increased stereotypic behaviour in response to the drug, increasing their stereotypic counts 2-fold following the administration of amphetamine at both doses (Figure 5c).
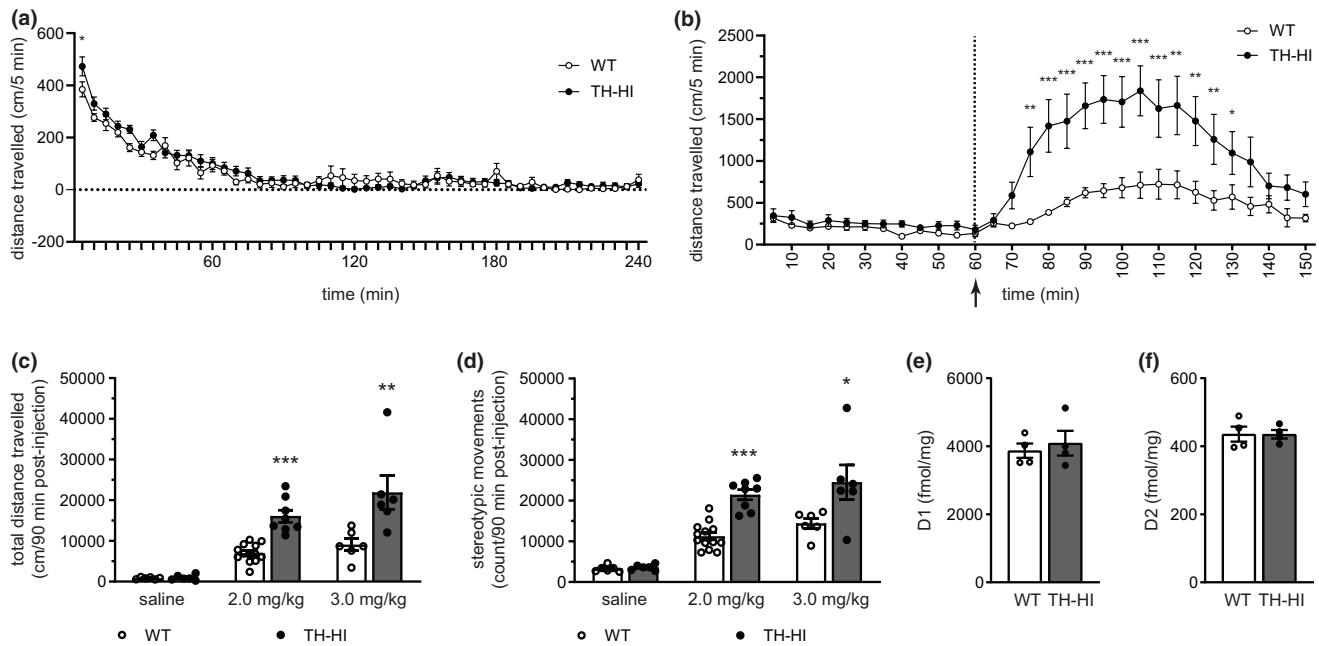
FIGURE 5 Locomotor response to amphetamine. (a) Baseline locomotor behaviour over 240 min, measured as total distance travelled (cm) in 5-min epochs. (Repeated-measures two-way ANOVA: effect of time, $F_{47, 987} = 65.20$, $p \leq .0001$; effect of genotype, $F_{1,987} = 0.39$, $p = .54$; genotype x drug interaction, $F_{47, 987} = 1.76$, $p \leq .0015$; Bonferroni post hoc) (WT $n = 12$, TH-HI $n = 11$). (b) Total distance travelled in 5-min epochs, before and after injection with 3.0 mg/kg amphetamine (arrow denotes time of injection). (Repeated-measures two-way ANOVA: effect of time, $F_{29,290} = 20.33$, $p \leq .0001$; effect of genotype, $F_{1,290} = 9.83$, $p = .011$; genotype x drug interaction, $F_{29,290} = 5.49$, $p \leq .0001$) (WT $n = 6$, TH-HI $n = 6$). (c) Total distance travelled in 90 min after injection of saline (Two-way ANOVA: effect of drug, $F_{2,39} = 35.36$, $p \leq .0001$; effect of genotype, $F_{1,39} = 28.45$, $p \leq .0001$; genotype x drug interaction, $F_{2,39} = 6.625$, $p = .0033$; Bonferroni post hoc) (saline: WT $n = 6$, TH-HI $n = 6$; 2.0 mg/kg: WT $n = 13$, TH-HI $n = 8$; 3 mg/kg: WT $n = 6$, TH-HI $n = 6$). (d) Total stereotypic counts in 90 min after injection of saline, 2.0 mg/kg, or 3.0 mg/kg amphetamine (multiple Mann–Whitney tests with the two-stage Benjamini, Krieger, and Yekutieli procedure) (saline: WT $n = 6$, TH-HI $n = 6$; 2.0 mg/kg: WT $n = 13$, TH-HI $n = 8$; 3 mg/kg: WT $n = 6$, TH-HI $n = 6$). (e) Quantification of striatal D1 receptors by radioligand binding ($n = 4$ per group; $p = .63$, t-test). (f) Quantification of striatal D2 receptors by radioligand binding ($n = 4$ per group; $p = .99$, t-test). n = number of mice. ($p \leq .05$, *, $p \leq .01$, **; $p \leq .001$, ***). Mean ± SEM

The potentiation in amphetamine-induced hyperactivity was not associated with alterations in dopamine D1 or D2 receptor levels in TH-HI mice (Figure 5e, f).

3.10 | Responses to amphetamine depend on dopamine synthesis

We next sought to confirm that the elevated amphetamine response seen in TH-HI mice resulted from de novo dopamine synthesis by using NSD1015, which blocks AADC. Administration of NDS-1015 had a significant drug effect, even during the pre-amphetamine habituation phase ($p = .013$, two-way ANOVA) (Figure S5a, b). In particular, during this habituation phase, TH-HI mice that had received NSD-1015 demonstrated reduced locomotor activity as compared with those that had received saline ($p \leq .05$, Tukey's multiple comparisons post hoc t-test).

Wild-type and TH-HI mice that had received NSD-1015 did not have a hyperactive response to amphetamine. After receiving an amphetamine challenge, total distance travelled by wild-type mice that had received an NSD-1015 pre-treatment was reduced by 77% of that travelled by wild-type mice that had received saline ($p < .01$,

Tukey's multiple comparisons post hoc t-test). Distance travelled by TH-HI mice that had received NSD-1015 was reduced by 97% of the distance travelled by TH-HI mice that had received the saline pre-treatment ($p < .0001$, Tukey's multiple comparisons post hoc t-test) (Figure S5b).

3.11 | TH-HI mice show increased sensitivity to methamphetamine toxicity

We next tested the sensitivity of TH-HI mice to methamphetamine toxicity. At doses of 5.0 mg/kg or 10 mg/kg, there was no difference in the hyperthermic response to methamphetamine between adult TH-HI mice and wild-type littermates (Figure 6a). At 48 hr after intraperitoneal injection of 5.0 mg/kg methamphetamine, mean DAT striatal protein levels were reduced by 62.2% in wild-type mice and 67.0% in TH-HI mice relative to saline-treated wild-type controls (Figure 6b, c). In response to 10 mg/kg, DAT levels were reduced by 65.2% in wild-type mice and 79.7% in TH-HI compared with DAT levels of saline-treated wild-type mice. The TH-HI group had greater sensitivity to methamphetamine than their wild-type littermates at the 10 mg/kg dose ($p \leq .05$, two-way ANOVA).
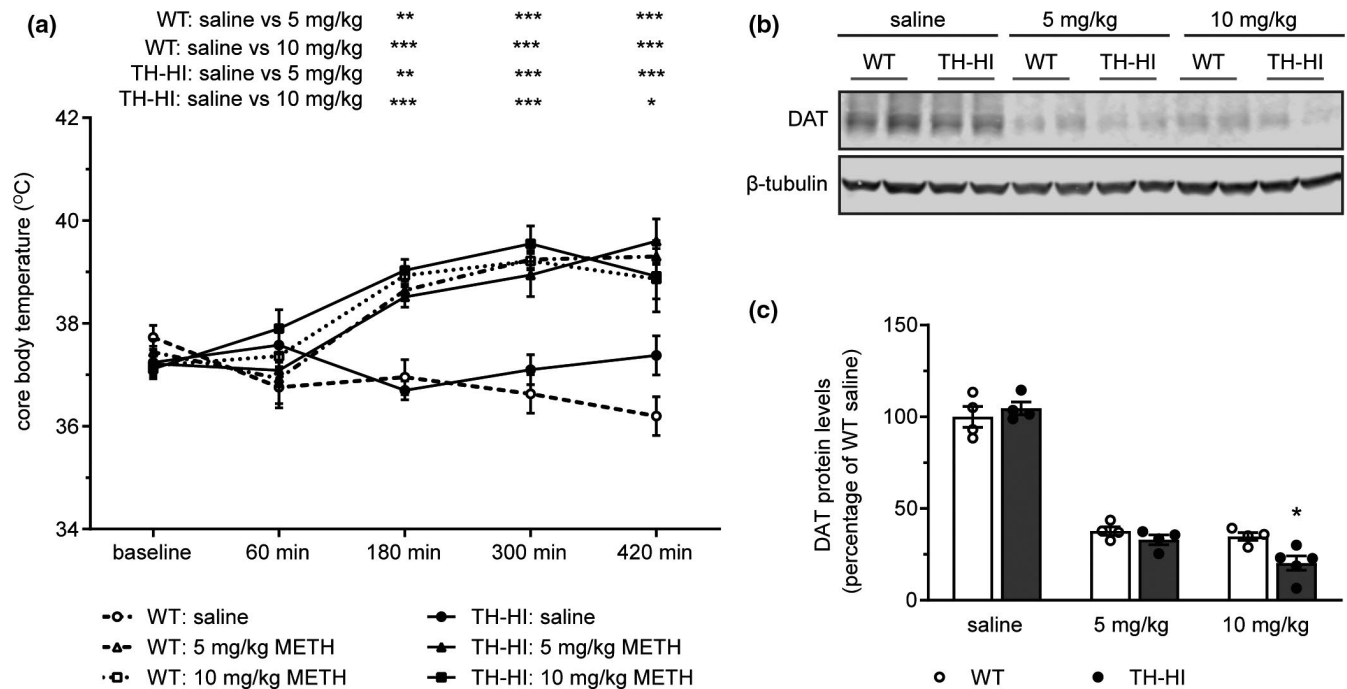
FIGURE 6 Toxicity of methamphetamine. (a) Measurements of the core body temperature of animals administered with saline, 5 mg/kg or 10 mg/kg of methamphetamine revealed no difference in the effect of treatment between genotypes. ($p \leq .05$, *; $p \leq .01$, **; $p \leq .001$, ***, repeated-measures two-way ANOVA) (WT: saline $n = 7$, 5 mg/kg $n = 7$, 10 mg/kg $n = 6$; TH-HI: saline $n = 5$, 5 mg/kg $n = 7$, 10 mg/kg $n = 6$). (b) Representative blot, showing striatal DAT protein levels in WT and TH-HI mice, ($n = 2$ of 4 shown per treatment group). (c) Striatal DAT protein levels relative to level seen in WT mice treated with saline, after administration of saline, 5 mg/kg or 10 mg/kg methamphetamine. (effect of genotype, ns; effect of dose, $F_{2, 19} = 255.4$, $p \leq .0001$; genotype × dose interaction, $F_{2, 19} = 3.59$, $p = .048$; two-way ANOVA) (Bonferroni post hoc, $p = .025$, *) $n =$ number of mice. Mean ± SEM

4 | DISCUSSION

Here we report that directly increasing TH activity in transgenic mice augments dopamine turnover and produces markers of oxidative stress in the striatum including elevated levels of H_2O_2, associated with accumulation of the autotoxic catecholamine metabolites DOPAL and Cys-DA. Increased dopamine production also results in increased susceptibility to amphetamine-induced hyperactivity and methamphetamine toxicity. These findings suggest that a loss of TH regulation could be one factor contributing to mounting oxidative stress in early-stage pathologies that is specific to catecholamine neurons.

TH-HI mice had a 3-fold increase in both mRNA and total TH protein levels (Figure 2c,d, f, g). In addition, transgenic mice had approximately 3 times the levels of phosphorylated TH (Figure S2) and increased rates of TH activity compared with age-matched littermates (Figure 3a). Phosphorylation of TH directly influences the rate of catecholamine synthesis by inducing a conformational change that releases the enzyme from end-product inhibition—a state in which a newly synthesized catechol is bound to ferric (Fe^{3+}) iron in the active site of TH following a hydroxylation reaction. In turn, unbinding of catechols allows the iron molecule to be reduced to its ferrous (Fe^{2+}) form, returning TH to an active state and freeing the iron molecule for further interactions (Dunkley et al. 1996; Haavik, 1997; Haavik et al. 1997). Our findings show that TH-HI mice

have a significant increase in the levels of active-state TH compared with their non-transgenic littermates, in turn leading to increased dopamine production.

In TH-HI mice, the proportionate increase in striatal DOPAC content exceeded that of dopamine, indicating an increased rate of intracellular dopamine turnover (Figure 3d) (Gemechu et al. 2018). Under normal circumstances, the majority of the catecholamine pool is stored in vesicles, rendering it available for release upon neuronal stimulation and protecting the cell from oxidative processes that could be damaging (Pifl et al. 2014; Taylor et al. 2014; Vernon, 2009). Increased VMAT2 levels have been shown to lead to increased size and filling of presynaptic vesicles (Lohr et al. 2014, 2015), and thus, an up-regulation in VMAT2 expression could reflect a strategy by which cells might mitigate damage induced by an increased presence of monoamines in the cytosol. TH-HI mice did not differ from wild-type littermates in VMAT2 levels (Figure S3) and therefore may not have compensated adequately for the increase in dopamine production. Consistent with this finding, TH-HI mice showed an increase in striatal H_2O_2 concomitant with decreased striatal glutathione and increased DOPAL content (Figure 4).

A recent study by Bucher et al. (2020) that examined the critical role of VMAT2 in maintaining dopamine homeostasis further emphasizes the toxicity of rising levels of cytosolic dopamine. An adeno-associated virus was used to introduce small-hairpin RNA

interference of endogenous VMAT2 in adult rats, resulting in a progressive adult-onset loss of VMAT2 and accumulation of unsequestered dopamine. The disruption resulted in a subsequent increase in dopamine metabolism, behavioural deficits and degeneration of nigrostriatal neurons—consequences that were rescued through the reintroduction of VMAT2 (Bucher et al. 2020). These results show that dysregulation of dopamine homeostasis acquired in adulthood is sufficient to produce dopamine toxicity in the nigrostriatal pathway (Bucher et al. 2020).

Dopamine dysregulation can promote cytotoxicity due to the potential for oxidation (Caudle et al. 2007; Chen et al. 2008; Hastings et al. 1996; Masoud et al. 2015; Mosharov et al. 2009; Taylor et al. ,2009, 2014). DOPAL and H_2O_2 are formed as a result of the enzymatic metabolism of dopamine (Goldstein et al. 2013; Spina & Cohen, 1989). DOPAL itself also spontaneously oxidizes forming DOPAL-quinones, and in the process generates superoxide radicals. These radicals are believed to contribute to DOPAL-induced oligomerization of α-synuclein (Werner-Allen et al. 2017), impede vesicular functions (Plotegher et al. 2017), and damage mitochondrial function (Sarafian et al. 2019). DOPAL-quinones are capable of forming protein adducts with α-synuclein and other intracellular proteins, which can in turn initiate cytotoxic processes (Jinsmaa et al. 2018).

In addition to producing damaging compounds through the process of metabolism, unsequestered dopamine and related compounds are susceptible to spontaneous oxidation, forming ROS and dopamine-quinones. Dopamine-quinones—which are electron-deficient—can then react with reduced sulfhydryl groups such as free cysteine or glutathione, or covalently bind to cysteine groups on nucleophilic proteins (often at the active site), which can impair their function and have detrimental effects on the cell (Goldstein et al. 2016, 2017; Hastings et al. 1996; Hastings & Zigmond, 1994). Therefore, the presence of cysteinylated catechols is used as a measure of the oxidation of free cytosolic dopamine (Caudle et al. 2007; Chen et al. 2008; Masoud et al. 2015). TH-HI mice had elevated levels of DOPAL as well as increased levels of cysteinyl-L-DOPA and cysteinyl-dopamine (Figure 4), providing evidence of both enzymatic and spontaneous oxidation (Figure S6) (Chen et al. 2008; Fornstedt et al. 1989, 1990; Fornstedt & Carlsson, 1989; Hastings et al. 1996).

Recent studies suggest a critical link between unsequestered catecholamines and α-synuclein aggregation, leading to toxicity. Alpha-synuclein oligomers have been shown to be kinetically stabilized by oxidized dopamine and other catecholamines in vitro (Conway et al. 2001; Mor et al. 2017; Norris & Giasson, 2005; Norris et al. 2005). Mor et al. (2017) reported that chronic elevation of dopamine levels in α-synuclein A53T mice results in progressive nigrostriatal degeneration and locomotor impairment, to an extent not seen in A53T mice alone, demonstrating a synergistic toxicity of dopamine and α-synuclein. Dopamine was also shown to modify α-synuclein aggregation in vivo, forming oligomers that share biochemical and structural characteristics with neurotoxic α-synuclein oligomers produced by interactions with dopamine in vitro (Mor et al. 2017). In another study, Burbulla et al. (2017)

causally linked lysosomal dysfunction and α-synuclein accumulation to elevated levels of oxidized dopamine in the cytosol, in a dopamine-dependent "toxic cascade," using dopamine neurons derived from Parkinson's patients (Burbulla et al. 2017). In cultured human oligodendrocytes and PC12 rat pheochromocytoma cells, Jinsmaa et al. demonstrated that DOPAL is even more potent than dopamine in producing quinones and protein modifications, including the oligomerization of α-synuclein. Notably, treatment with the antioxidant N-acetylcysteine—a precursor of glutathione— reduced DOPAL-quinone formation, in turn attenuating or preventing all associated protein modifications (including α-synuclein oligomerization) (Jinsmaa et al. 2018).

TH-HI mice also showed an increase in the hyperactive response to amphetamine (Figure 5). This response was dependent on de novo dopamine synthesis (Supp. Figure 5). Amphetamine releases dopamine from vesicles and causes a rapid efflux of cytosolic dopamine into the extracellular space due to backward transport through the cell membrane dopamine transporter (Masoud et al. 2015; Takahashi et al. 1997). Similarly, methamphetamine can redistribute dopamine from intraneuronal storage sites and in this way is believed to result in increased dopamine auto-oxidation and dopamine terminal injury (Fumagalli et al. 1998). Our finding that TH-HI mice had augmented sensitivity to methamphetamine toxicity is consistent with an additive effect on an already-elevated basal state of oxidative stress (Figure 6).

How an increase in TH activity might specifically contribute to oxidative stress in vivo is of particular relevance, as past studies have shown diminished TH regulation to coincide with other pathological change, such as increased α-synuclein aggregation (Alerte et al. 2008; Farrell et al. 2014; Greenwood et al. 1991; Liu et al. 2015; Liu, Zhang, et al., 2008; Locke et al. 2008; Lou et al. 2010; Walker et al. 2013; Zhou et al. 2011). Although Parkinson's disease and ageing are associated with dopaminergic cell loss—and thus, a loss of TH-positive cells—past studies showed that in C57BL mice aged 104 weeks, striatal DA and DOPAC contents were 5–7 times higher in surviving TH-positive substantia nigra pars compacta neurons compared with those in 8-week-old mice, suggesting that surviving neurons compensate for the neuronal loss by increasing dopamine synthesis (Greenwood et al. 1991). Similar results have been seen in MPTP-treated mice, where there is a compensatory increase in TH activity in the remaining individual surviving neurons (Greenwood et al. 1991; Kozina et al. 2014). Therefore, particularly as other pathologies emerge, it is possible that TH might contribute to mounting oxidative stress if activity is considered at the level of the cell.

TH-HI mice may be a useful model for further investigating catecholamine autotoxicity in the context of Parkinson's disease, particularly as it relates to α-synuclein modifications and dopaminergic cell death. First, oxidation products are known to stabilize α-synuclein oligomers (Conway et al. 2001; Mor et al. 2017), which have a diminished ability to regulate TH activity (Hua et al. 2015; Lou et al. 2010; Park et al. 2016; Peng et al. 2005; Wu et al. 2011). Therefore, it is possible that the products of spontaneous and metabolically oxidized dopamine in turn impede the regulation of

dopamine production, producing a pathogenic cycle that further facilitates dopamine dysregulation. Second, DOPAL-induced protein modifications such as α-synuclein oligomerization can in turn impede vesicular functions, which may lead to increased levels of cytosolic dopamine (Goldstein, 2020; Masato et al. 2019; Plotegher et al. 2017). Again, this could result in the genesis of a cytotoxic cycle. Many recent studies have indeed suggested that oxidized dopamine and α-synuclein oligomers are together engaged in pathogenesis and the degeneration of dopaminergic cells (Burbulla et al. 2017; Lou et al. 2010; Mor et al. 2017; Qu et al. 2018), and such pathways could be explored in future studies using TH-HI mice.

In conclusion, directly increasing TH activity alone is sufficient to produce markers of oxidative stress, such as increased striatal H_2O_2 and a decreased glutathione level. TH-HI mice have neurochemical evidence for increases in both enzymatic and spontaneous oxidation of cytoplasmic dopamine, as indicated by increased levels of DOPAL and 5-S-cysteinyldopamine. Altered TH regulation due to age or early-stage pathologies could be one factor contributing to mounting oxidative stress, and support further studies of TH as a potential contributor to catecholamine dysregulation.

CONFLICTS OF INTEREST

Dr Shababa T. Masoud is now employed at Denali Therapeutics (San Francisco, CA, USA). There are no other potential conflicts of interest to report.

AUTHORS CONTRIBUTIONS

Laura M. Vecchio: experimental design, execution of experiments, data analysis and figure preparation, manuscript preparation, and manuscript revisions; Patricia Sullivan, Amy R. Dunn, Marie Kristel Bermejo, Rong Fu, Shababa T. Masoud, and Emil Gregersen: execution of experiment, manuscript editing; Nikhil M. Urs and Reza Nazari: execution of experiment; Poul Henning Jensen: contributed reagents, experimental design, manuscript editing; Amy Ramsey and Ali Salahpour: executed experiments, contributed reagents, experimental design, manuscript editing; David S. Goldstein: contributed reagents, experimental design, experimental data, manuscript editing; Gary W. Miller: contributed reagents, experimental design, manuscript editing.

OPEN RESEARCH BADGES

This article has earned Open Data and Open Materials badges (see https://cos.io/our-services/open-science-badges/ for more information). A Preprint of this article has been posted on https://www.biorxiv.org/content/10.1101/188318v1.

DATA AVAILABILITY STATEMENT

The data that support the findings of this study are available from the corresponding author upon reasonable request. Unaltered Western blots and immunohistochemistry images are available at Open Science Framework (https://osf.io). Western blots: https://osf.io/3sj6v/?view_only=c580d782a77d475984bb35eb41738279; Immunohistochemistry: https://osf.io/2tqwe/?view_only=c9d0d187221c4ca989bc93455534b98d

ORCID

Laura M. Vecchio https://orcid.org/0000-0003-1520-9336
Amy R. Dunn https://orcid.org/0000-0001-6437-6099
Emil Gregersen https://orcid.org/0000-0003-3923-4405
Nikhil M. Urs https://orcid.org/0000-0003-1819-7836
Poul Henning Jensen https://orcid.org/0000-0002-4439-9020
Amy Ramsey https://orcid.org/0000-0002-2717-5279
David S. Goldstein https://orcid.org/0000-0002-5709-9940
Gary W. Miller https://orcid.org/0000-0001-8984-1284

REFERENCES

Adams, J. D. Jr, Klaidman, L. K., & Ribeiro, P. (1997). Tyrosine hydroxylase: Mechanisms of oxygen radical formation. *Redox Report : Communications in Free Radical Research*, *3*, 273–279. https://doi.org/10.1080/13510002.1997.11747123

Alerte, T. N., Akinfolarin, A. A., Friedrich, E. E., Mader, S. A., Hong, C. S., & Perez, R. G. (2008). Alpha-synuclein aggregation alters tyrosine hydroxylase phosphorylation and immunoreactivity: Lessons from viral transduction of knockout mice. *Neuroscience Letters*, *435*, 24–29.

Anderson, D. G., Mariappan, S. V., Buettner, G. R., & Doorn, J. A. (2011). Oxidation of 3,4-dihydroxyphenylacetaldehyde, a toxic dopaminergic metabolite, to a semiquinone radical and an ortho-quinone. *Journal of Biological Chemistry*, *286*, 26978–26986.

Arawaka, S., Sato, H., Sasaki, A., Koyama, S., & Kato, T. (2017). Mechanisms underlying extensive Ser129-phosphorylation in alpha-synuclein aggregates. *Acta Neuropathologica Communications*, 5, 48.

Ballester, M., Castello, A., Ibanez, E., Sanchez, A., & Folch, J. M. (2004). Real-time quantitative PCR-based system for determining transgene copy number in transgenic animals. *BioTechniques*, 37, 610–613. https://doi.org/10.2144/04374ST06

Bernstein, A. I., Stout, K. A., & Miller, G. W. (2014). The vesicular monoamine transporter 2: An underexplored pharmacological target. *Neurochemistry International*, 73, 89–97. https://doi.org/10.1016/j.neuint.2013.12.003

Bisaglia, M., Tosatto, L., Munari, F., Tessari, I., de Laureto, P. P., Mammi, S., & Bubacco, L. (2010). Dopamine quinones interact with alpha-synuclein to form unstructured adducts. *Biochemical and Biophysical Research Communications*, 394, 424–428.

Blesa, J., Trigo-Damas, I., Quiroga-Varela, A., & Jackson-Lewis, V. R. (2015). Oxidative stress and Parkinson's disease. *Frontiers in Neuroanatomy*, 9, 91. https://doi.org/10.3389/fnana.2015.00091

Bolam, J. P., & Pissadaki, E. K. (2012). Living on the edge with too many mouths to feed: Why dopamine neurons die. *Movement Disorders*, 27, 1478–1483. https://doi.org/10.1002/mds.25135

Braak, H., Del Tredici, K., Rub, U., de Vos, R. A., Jansen Steur, E. N., & Braak, E. (2003). Staging of brain pathology related to sporadic Parkinson's disease. *Neurobiology of Aging*, 24, 197–211. https://doi.org/10.1016/S0197-4580(02)00065-9

Bucher, M. L., Barrett, C. W., Moon, C. J., Mortimer, A. D., Burton, E. A., Timothy Greenamyre, J., & Hastings, T. G. (2020). Acquired dysregulation of dopamine homeostasis reproduces features of Parkinson's disease. *npj Parkinson's Disease*, 6, 34. https://doi.org/10.1038/s41531-020-00134-x

Burbulla, L. F., Song, P., Mazzulli, J. R., Zampese, E., Wong, Y. C., Jeon, S., Santos, D. P., Blanz, J., Obermaier, C. D., Strojny, C., Savas, J. N., Kiskinis, E., Zhuang, X., Krüger, R., Surmeier, D. J., & Krainc, D. (2017). Dopamine oxidation mediates mitochondrial and lysosomal dysfunction in Parkinson's disease. *Science*, 357, 1255–1261. https://doi.org/10.1126/science.aam9080

Burke, W. J., Kumar, V. B., Pandey, N., Panneton, W. M., Gan, Q., Franko, M. W., O'Dell, M., Li, S. W., Pan, Y., Chung, H. D., & Galvin, J. E. (2008). Aggregation of α-synuclein by DOPAL, the monoamine oxidase metabolite of dopamine. *Acta Neuropathologica*, 115(2), 193–203. https://doi.org/10.1007/s00401-007-0303-9

Burkhart, C. A., Norris, M. D., & Haber, M. (2002). A simple method for the isolation of genomic DNA from mouse tail free of real-time PCR inhibitors. *Journal of Biochemical and Biophysical Methods*, 52, 145–149. https://doi.org/10.1016/S0165-022X(02)00052-0

Casida, J. E., Ford, B., Jinsmaa, Y., Sullivan, P., Cooney, A., & Goldstein, D. S. (2014). Benomyl, aldehyde dehydrogenase, DOPAL, and the catecholaldehyde hypothesis for the pathogenesis of Parkinson's disease. *Chemical Research in Toxicology*, 27, 1359–1361. https://doi.org/10.1021/tx5002223

Caudle, W. M., Richardson, J. R., Wang, M. Z., Taylor, T. N., Guillot, T. S., McCormack, A. L., Colebrooke, R. E., Di Monte, D. A., Emson, P. C., & Miller, G. W. (2007). Reduced vesicular storage of dopamine causes progressive nigrostriatal neurodegeneration. *Journal of Neuroscience*, 27, 8138–8148. https://doi.org/10.1523/JNEUROSCI.0319-07.2007

Chen, L., Ding, Y., Cagniard, B., Van Laar, A. D., Mortimer, A., Chi, W., Hastings, T. G., Kang, U. J., & Zhuang, X. (2008). Unregulated cytosolic dopamine causes neurodegeneration associated with oxidative stress in mice. *Journal of Neuroscience*, 28, 425–433. https://doi.org/10.1523/JNEUROSCI.3602-07.2008

Chen, M., Yang, W., Li, X., Li, X., Wang, P., Yue, F., Yang, H., Chan, P., & Yu, S. (2016). Age- and brain region-dependent alpha-synuclein oligomerization is attributed to alterations in intrinsic enzymes regulating alpha-synuclein phosphorylation in aging monkey brains. *Oncotarget*, 7, 8466–8480.

Cliburn, R. A., Dunn, A. R., Stout, K. A., Hoffman, C. A., Lohr, K. M., Bernstein, A. I., Winokur, E. J., Burkett, J., Schmitz, Y., Caudle, W. M., & Miller, G. W. (2017). Immunochemical localization of vesicular monoamine transporter 2 (VMAT2) in mouse brain. *Journal of Chemical Neuroanatomy*, 83–84, 82–90. https://doi.org/10.1016/j.jchemneu.2016.11.003

Conway, K. A., Rochet, J. C., Bieganski, R. M., & Lansbury, P. T. Jr (2001). Kinetic stabilization of the alpha-synuclein protofibril by a dopamine-alpha-synuclein adduct. *Science*, 294, 1346–1349. https://doi.org/10.1126/science.1063522

Dalle-Donne, I., Rossi, R., Giustarini, D., Milzani, A., & Colombo, R. (2003). Protein carbonyl groups as biomarkers of oxidative stress. *Clinica Chimica Acta*, 329(1–2), 23–38. https://doi.org/10.1016/s0009-8981(03)00003-2

Darvas, M., Henschen, C. W., & Palmiter, R. D. (2014). Contributions of signaling by dopamine neurons in dorsal striatum to cognitive behaviors corresponding to those observed in Parkinson's disease. *Neurobiology of Diseases*, 65, 112–123. https://doi.org/10.1016/j.nbd.2014.01.017

Daubner, S. C., Le, T., & Wang, S. (2011). Tyrosine hydroxylase and regulation of dopamine synthesis. *Archives of Biochemistry and Biophysics*, 508, 1–12. https://doi.org/10.1016/j.abb.2010.12.017

de Diego, A. M., Gandia, L., & Garcia, A. G. (2008). A physiological view of the central and peripheral mechanisms that regulate the release of catecholamines at the adrenal medulla. *Acta Physiologica*, 192, 287–301. https://doi.org/10.1111/j.1748-1716.2007.01807.x

de Freitas, C. M., Busanello, A., Schaffer, L. F., Peroza, L. R., Krum, B. N., Leal, C. Q., Ceretta, A. P., da Rocha, J. B., & Fachinetto, R. (2016). Behavioral and neurochemical effects induced by reserpine in mice. *Psychopharmacology (Berl)*, 233, 457–467. https://doi.org/10.1007/s00213-015-4118-4

Del Tredici, K., & Braak, H. (2013). Dysfunction of the locus coeruleus-norepinephrine system and related circuitry in Parkinson's disease-related dementia. *Journal of Neurology, Neurosurgery and Psychiatry*, 84, 774–783.

Dunkley, P. R., Bobrovskaya, L., Graham, M. E., von Nagy-Felsobuki, E. I., & Dickson, P. W. (2004). Tyrosine hydroxylase phosphorylation: Regulation and consequences. *Journal of Neurochemistry*, 91, 1025–1043. https://doi.org/10.1111/j.1471-4159.2004.02797.x

Dunkley, P. R., Cote, A., Harrison, S. M., Herd, L., Hall, A., & Powis, D. A. (1996). Tyrosine hydroxylase phosphorylation in bovine adrenal chromaffin cells. Clonidine stimulates basal but inhibits nicotinic receptor evoked phosphorylation. *Biochemical Pharmacology*, 51, 239–245. https://doi.org/10.1016/0006-2952(95)02128-0

Dunkley, P. R., & Dickson, P. W. (2019). Tyrosine hydroxylase phosphorylation in vivo. *Journal of Neurochemistry*, 149, 706–728.

Fahn, S. (2003). Description of Parkinson's disease as a clinical syndrome. *Annals of the New York Academy of Sciences*, 991, 1–14. https://doi.org/10.1111/j.1749-6632.2003.tb07458.x

Farrell, K. F., Krishnamachari, S., Villanueva, E., Lou, H., Alerte, T. N., Peet, E., Drolet, R. E., & Perez, R. G. (2014). Non-motor parkinsonian pathology in aging A53T alpha-synuclein mice is associated with progressive synucleinopathy and altered enzymatic function. *Journal of Neurochemistry*, 128, 536–546.

Ferris, M. J., Espana, R. A., Locke, J. L., Konstantopoulos, J. K., Rose, J. H., Chen, R., & Jones, S. R. (2014). Dopamine transporters govern diurnal variation in extracellular dopamine tone. *Proceedings of the National Academy of Sciences*, 111, E2751–2759. https://doi.org/10.1073/pnas.1407935111

Fitzmaurice, A. G., Rhodes, S. L., Lulla, A., Murphy, N. P., Lam, H. A., O'Donnell, K. C., Barnhill, L., Casida, J. E., Cockburn, M., Sagasti, A., Stahl, M. C., Maidment, N. T., Ritz, B., & Bronstein, J. M. (2013). Aldehyde dehydrogenase inhibition as a pathogenic mechanism in Parkinson disease. *Proceedings of the National Academy of Sciences*, 110, 636–641. https://doi.org/10.1073/pnas.1220399110

Follmer, C., Coelho-Cerqueira, E., Yatabe-Franco, D. Y., Araujo, G. D., Pinheiro, A. S., Domont, G. B., & Eliezer, D. (2015). Oligomerization and membrane-binding properties of covalent adducts formed by the interaction of alpha-synuclein with the toxic dopamine metabolite 3,4-dihydroxyphenylacetaldehyde (DOPAL). *Journal of Biological Chemistry*, *290*, 27660–27679.

Fornstedt, B., Brun, A., Rosengren, E., & Carlsson, A. (1989). The apparent autoxidation rate of catechols in dopamine-rich regions of human brains increases with the degree of depigmentation of substantia nigra. *Journal of neural transmission. Parkinson's Disease and Dementia Section*, *1*, 279–295.

Fornstedt, B., & Carlsson, A. (1989). A marked rise in 5-S-cysteinyl-dopamine levels in guinea-pig striatum following reserpine treatment. *Journal of Neural Transmission*, *76*, 155–161. https://doi.org/10.1007/BF01578755

Fornstedt, B., Pileblad, E., & Carlsson, A. (1990). In vivo autoxidation of dopamine in guinea pig striatum increases with age. *Journal of Neurochemistry*, *55*, 655–659. https://doi.org/10.1111/j.1471-4159.1990.tb04183.x

Fumagalli, F., Gainetdinov, R. R., Valenzano, K. J., & Caron, M. G. (1998). Role of dopamine transporter in methamphetamine-induced neurotoxicity: Evidence from mice lacking the transporter. *Journal of Neuroscience*, *18*, 4861–4869. https://doi.org/10.1523/JNEUROSCI.18-13-04861.1998

Gemechu, J. M., Sharma, A., Yu, D., Xie, Y., Merkel, O. M., & Moszczynska, A. (2018). Characterization of dopaminergic system in the striatum of young adult Park2(-/-) knockout rats. *Scientific Reports*, *8*, 1517. https://doi.org/10.1038/s41598-017-18526-0

Ghisi, V., Ramsey, A. J., Masri, B., Gainetdinov, R. R., Caron, M. G., & Salahpour, A. (2009). Reduced D2-mediated signaling activity and trans-synaptic upregulation of D1 and D2 dopamine receptors in mice overexpressing the dopamine transporter. *Cellular Signalling*, *21*, 87–94. https://doi.org/10.1016/j.cellsig.2008.09.011

Giros, B., Jaber, M., Jones, S. R., Wightman, R. M., & Caron, M. G. (1996). Hyperlocomotion and indifference to cocaine and amphetamine in mice lacking the dopamine transporter. *Nature*, *379*, 606–612. https://doi.org/10.1038/379606a0

Goldstein, D. S. (2020). Correction to: The catecholaldehyde hypothesis: Where MAO fits in. *Journal of Neural Transmission*, *127*, 179. https://doi.org/10.1007/s00702-019-02128-3

Goldstein, D. S., Jinsmaa, Y., Sullivan, P., Holmes, C., Kopin, I. J., & Sharabi, Y. (2016). Comparison of monoamine oxidase inhibitors in decreasing production of the autotoxic dopamine metabolite 3,4-dihydroxyphenylacetaldehyde in PC12 cells. *Journal of Pharmacology and Experimental Therapeutics*, *356*, 483–492. https://doi.org/10.1124/jpet.115.230201

Goldstein, D. S., Jinsmaa, Y., Sullivan, P., & Sharabi, Y. (2017). N-acetylcysteine prevents the increase in spontaneous oxidation of dopamine during monoamine oxidase inhibition in PC12 cells. *Neurochemical Research*, *42*, 3289–3295. https://doi.org/10.1007/s11064-017-2371-0

Goldstein, D. S., Kopin, I. J., & Sharabi, Y. (2014). Catecholamine autotoxicity. Implications for pharmacology and therapeutics of Parkinson disease and related disorders. *Pharmacology & Therapeutics*, *144*, 268–282.

Goldstein, D. S., Sharabi, Y., Karp, B. I., Bentho, O., Saleem, A., Pacak, K., & Eisenhofer, G. (2007). Cardiac sympathetic denervation preceding motor signs in Parkinson disease. *Clinical Autonomic Research: Official Journal of the Clinical Autonomic Research Society*, *17*, 118–121. https://doi.org/10.1007/s10286-007-0396-1

Goldstein, D. S., Sullivan, P., Holmes, C., Miller, G. W., Alter, S., Strong, R., Mash, D. C., Kopin, I. J., & Sharabi, Y. (2013). Determinants of buildup of the toxic dopamine metabolite DOPAL in Parkinson's disease. *Journal of Neurochemistry*, *126*, 591–603. https://doi.org/10.1111/jnc.12345

Graham, D. G. (1978). Oxidative pathways for catecholamines in the genesis of neuromelanin and cytotoxic quinones. *Molecular Pharmacology*, *14*, 633–643.

Greenwood, C. E., Tatton, W. G., Seniuk, N. A., & Biddle, F. G. (1991). Increased dopamine synthesis in aging substantia nigra neurons. *Neurobiology of Aging*, *12*, 557–565. https://doi.org/10.1016/0197-4580(91)90087-Z

Haavik, J. (1997). L-DOPA is a substrate for tyrosine hydroxylase. *Journal of Neurochemistry*, *69*, 1720–1728.

Haavik, J., Almas, B., & Flatmark, T. (1997). Generation of reactive oxygen species by tyrosine hydroxylase: A possible contribution to the degeneration of dopaminergic neurons? *Journal of Neurochemistry*, *68*, 328–332. https://doi.org/10.1046/j.1471-4159.1997.68010328.x

Haavik, J., Schelling, D. L., Campbell, D. G., Andersson, K. K., Flatmark, T., & Cohen, P. (1989). Identification of protein phosphatase 2A as the major tyrosine hydroxylase phosphatase in adrenal medulla and corpus striatum: Evidence from the effects of okadaic acid. *FEBS Letters*, *251*, 36–42. https://doi.org/10.1016/0014-5793(89)81424-3

Hastings, T. G., Lewis, D. A., & Zigmond, M. J. (1996). Role of oxidation in the neurotoxic effects of intrastriatal dopamine injections. *Proceedings of the National Academy of Sciences*, *93*, 1956–1961. https://doi.org/10.1073/pnas.93.5.1956

Hastings, T. G., & Zigmond, M. J. (1994). Identification of catechol-protein conjugates in neostriatal slices incubated with [3H]dopamine: Impact of ascorbic acid and glutathione. *Journal of Neurochemistry*, *63*, 1126–1132. https://doi.org/10.1046/j.1471-4159.1994.63031126.x

Haycock, J. W., Lew, J. Y., Garcia-Espana, A., Lee, K. Y., Harada, K., Meller, E., & Goldstein, M. (1998). Role of serine-19 phosphorylation in regulating tyrosine hydroxylase studied with site- and phosphospecific antibodies and site-directed mutagenesis. *Journal of Neurochemistry*, *71*, 1670–1675. https://doi.org/10.1046/j.1471-4159.1998.71041670.x

Heal, D. J., Smith, S. L., Gosden, J., & Nutt, D. J. (2013). Amphetamine, past and present–a pharmacological and clinical perspective. *Journal of Psychopharmacology*, *27*, 479–496. https://doi.org/10.1177/0269881113482532

Hermida-Ameijeiras, A., Mendez-Alvarez, E., Sanchez-Iglesias, S., Sanmartin-Suarez, C., & Soto-Otero, R. (2004). Autoxidation and MAO-mediated metabolism of dopamine as a potential cause of oxidative stress: Role of ferrous and ferric ions. *Neurochemistry International*, *45*, 103–116. https://doi.org/10.1016/j.neuint.2003.11.018

Hu, Y. F., Caron, M. G., & Sieber-Blum, M. (2009). Norepinephrine transport-mediated gene expression in noradrenergic neurogenesis. *BMC Genomics*, *10*, 151. https://doi.org/10.1186/1471-2164-10-151

Hua, G., Xiaolei, L., Weiwei, Y., Hao, W., Yuangang, Z., Dongmei, L., Yazhuo, Z., & Hui, Y. (2015). Protein phosphatase 2A is involved in the tyrosine hydroxylase phosphorylation regulated by alpha-synuclein. *Neurochemical Research*, *40*, 428–437.

Jinsmaa, Y., Isonaka, R., Sharabi, Y., & Goldstein, D. S. (2020). 3,4-dihydroxyphenylacetaldehyde is more efficient than dopamine in oligomerizing and quinonizing alpha-synuclein. *Journal of Pharmacology and Experimental Therapeutics*, *372*, 157–165.

Jinsmaa, Y., Sharabi, Y., Sullivan, P., Isonaka, R., & Goldstein, D. S. (2018). 3,4-dihydroxyphenylacetaldehyde-induced protein modifications and their mitigation by N-acetylcysteine. *Journal of Pharmacology and Experimental Therapeutics*, *366*, 113–124.

Jones, S. R., Gainetdinov, R. R., Jaber, M., Giros, B., Wightman, R. M., & Caron, M. G. (1998). Profound neuronal plasticity in response to inactivation of the dopamine transporter. *Proceedings of the National Academy of Sciences*, *95*, 4029–4034. https://doi.org/10.1073/pnas.95.7.4029

Jones, S. R., Gainetdinov, R. R., Wightman, R. M., & Caron, M. G. (1998). Mechanisms of amphetamine action revealed in mice lacking the

dopamine transporter. *Journal of Neuroscience*, *18*, 1979–1986. https://doi.org/10.1523/JNEUROSCI.18-06-01979.1998

Kaneda, N., Sasaoka, T., Kobayashi, K., Kiuchi, K., Nagatsu, I., Kurosawa, Y., Fujita, K., Yokoyama, M., Nomura, T., Katsuki, M., & Nagatsu, T. (1991). Tissue-specific and high-level expression of the human tyrosine hydroxylase gene in transgenic mice. *Neuron*, *6*, 583–594. https://doi.org/10.1016/0896-6273(91)90061-4

Kish, S. J., Shannak, K., & Hornykiewicz, O. (1988). Uneven pattern of dopamine loss in the striatum of patients with idiopathic Parkinson's disease. Pathophysiologic and clinical implications. *New England Journal of Medicine*, *318*, 876–880.

Kostyn, K., Boba, A., Kostyn, A., Kozak, B., Starzycki, M., Kulma, A., & Szopa, J. (2020). Expression of the tyrosine hydroxylase gene from rat leads to oxidative stress in potato plants. *Antioxidants*, *9*(8), 717. https://doi.org/10.3390/antiox9080717

Kozina, E. A., Khakimova, G. R., Khaindrava, V. G., Kucheryanu, V. G., Vorobyeva, N. E., Krasnov, A. N., Georgieva, S. G., Kerkerian-Le Goff, L., & Ugrumov, M. V. (2014). Tyrosine hydroxylase expression and activity in nigrostriatal dopaminergic neurons of MPTP-treated mice at the presymptomatic and symptomatic stages of parkinsonism. *Journal of the Neurological Sciences*, *340*, 198–207. https://doi.org/10.1016/j.jns.2014.03.028

Lamensdorf, I., Hrycyna, C., He, L. P., Nechushtan, A., Tjurmina, O., Harvey-White, J., Eisenhofer, G., Rojas, E., & Kopin, I. J. (2000). Acidic dopamine metabolites are actively extruded from PC12 cells by a novel sulfonylurea-sensitive transporter. *Naunyn-Schmiedeberg's Archives of Pharmacology*, *361*, 654–664.

Lehmann, I. T., Bobrovskaya, L., Gordon, S. L., Dunkley, P. R., & Dickson, P. W. (2006). Differential regulation of the human tyrosine hydroxylase isoforms via hierarchical phosphorylation. *Journal of Biological Chemistry*, *281*, 17644–17651. https://doi.org/10.1074/jbc.M512194200

Li, H., & Dryhurst, G. (2001). Oxidative metabolites of 5-S-cysteinyldopamine inhibit the pyruvate dehydrogenase complex. *Journal of Neural Transmission*, *108*, 1363–1374. https://doi.org/10.1007/s007020100013

Li, S. W., Lin, T. S., Minteer, S., & Burke, W. J. (2001). 3,4-Dihydroxyphenylacetaldehyde and hydrogen peroxide generate a hydroxyl radical: Possible role in Parkinson's disease pathogenesis. *Brain Research. Molecular Brain Research*, *93*, 1–7. https://doi.org/10.1016/S0169-328X(01)00120-6

Lindgren, N., Xu, Z. Q., Lindskog, M., Herrera-Marschitz, M., Goiny, M., Haycock, J., Goldstein, M., Hokfelt, T., & Fisone, G. (2000). Regulation of tyrosine hydroxylase activity and phosphorylation at Ser(19) and Ser(40) via activation of glutamate NMDA receptors in rat striatum. *Journal of Neurochemistry*, *74*, 2470–2477. https://doi.org/10.1046/j.1471-4159.2000.0742470.x

Liu, D., Jin, L., Wang, H., Zhao, H., Zhao, C., Duan, C., Lu, L., Wu, B., Yu, S., Chan, P., Li, Y., & Yang, H. (2008). Silencing α-synuclein gene expression enhances tyrosine hydroxylase activity in MN9D cells. *Neurochemical Research*, *33*(7), 1401–1409. https://doi.org/10.1007/s11064-008-9599-7

Liu, G., Chen, M., Mi, N., Yang, W., Li, X., Wang, P., Yin, N., Li, Y., Yue, F., Chan, P., & Yu, S. (2015). Increased oligomerization and phosphorylation of α-synuclein are associated with decreased activity of glucocerebrosidase and protein phosphatase 2A in aging monkey brains. *Neurobiology of Aging*, *36*(9), 2649–2659. https://doi.org/10.1016/j.neurobiolaging.2015.06.004

Liu, G. P., Zhang, Y., Yao, X. Q., Zhang, C. E., Fang, J., Wang, Q., & Wang, J. Z. (2008). Activation of glycogen synthase kinase-3 inhibits protein phosphatase-2A and the underlying mechanisms. *Neurobiology of Aging*, *29*, 1348–1358. https://doi.org/10.1016/j.neurobiolaging.2007.03.012

Livak, K. J., & Schmittgen, T. D. (2001). Analysis of relative gene expression data using real-time quantitative PCR and the 2(-Delta Delta C(T)) Method. *Methods*, *25*, 402–408.

Locke, C. J., Fox, S. A., Caldwell, G. A., & Caldwell, K. A. (2008). Acetaminophen attenuates dopamine neuron degeneration in animal models of Parkinson's disease. *Neuroscience Letters*, *439*, 129–133. https://doi.org/10.1016/j.neulet.2008.05.003

Lohr, K. M., Bernstein, A. I., Stout, K. A., Dunn, A. R., Lazo, C. R., Alter, S. P., Wang, M., Li, Y., Fan, X., Hess, E. J., Yi, H., Vecchio, L. M., Goldstein, D. S., Guillot, T. S., Salahpour, A., & Miller, G. W. (2014). Increased vesicular monoamine transporter enhances dopamine release and opposes Parkinson disease-related neurodegeneration in vivo. *Proceedings of the National Academy of Sciences*, *111*, 9977–9982. https://doi.org/10.1073/pnas.1402134111

Lohr, K. M., Stout, K. A., Dunn, A. R., Wang, M., Salahpour, A., Guillot, T. S., & Miller, G. W. (2015). Increased vesicular monoamine transporter 2 (VMAT2; Slc18a2) protects against methamphetamine toxicity. *ACS Chemical Neuroscience*, *6*, 790–799.

Lou, H., Montoya, S. E., Alerte, T. N.M., Wang, J., Wu, J., Peng, X., Hong, C.-S., Friedrich, E. E., Mader, S. A., Pedersen, C. J., Marcus, B. S., McCormack, A. L., Di Monte, D. A., Daubner, S. C., & Perez, R. G. (2010). Serine 129 phosphorylation reduces the ability of α-synuclein to regulate tyrosine hydroxylase and protein phosphatase 2A in vitro and in vivo. *Journal of Biological Chemistry*, *285*(23), 17648–17661. https://doi.org/10.1074/jbc.m110.100867

Masato, A., Plotegher, N., Boassa, D., & Bubacco, L. (2019). Impaired dopamine metabolism in Parkinson's disease pathogenesis. *Molecular Neurodegeneration*, *14*, 35. https://doi.org/10.1186/s13024-019-0332-6

Masoud, S. T., Vecchio, L. M., Bergeron, Y., Hossain, M. M., Nguyen, L. T., Bermejo, M. K., Kile, B., Sotnikova, T. D., Siesser, W. B., Gainetdinov, R. R., Wightman, R. M., Caron, M. G., Richardson, J. R., Miller, G. W., Ramsey, A. J., Cyr, M., & Salahpour, A. (2015). Increased expression of the dopamine transporter leads to loss of dopamine neurons, oxidative stress and l-DOPA reversible motor deficits. *Neurobiology of Diseases*, *74*, 66–75. https://doi.org/10.1016/j.nbd.2014.10.016

Miyazaki, I., & Asanuma, M. (2008). Dopaminergic neuron-specific oxidative stress caused by dopamine itself. *Acta Medica Okayama*, *62*, 141–150.

Montine, T. J., Picklo, M. J., Amarnath, V., Whetsell, W. O. Jr, & Graham, D. G. (1997). Neurotoxicity of endogenous cysteinylcatechols. *Experimental Neurology*, *148*, 26–33.

Mor, D. E., Tsika, E., Mazzulli, J. R., Gould, N. S., Kim, H., Daniels, M. J., Doshi, S., Gupta, P., Grossman, J. L., Tan, V. X., Kalb, R. G., Caldwell, K. A, Caldwell, G. A., Wolfe, J. H., & Ischiropoulos, H. (2017). Dopamine induces soluble α-synuclein oligomers and nigrostriatal degeneration. *Nature Neuroscience*, *20*(11), 1560–1568. https://doi.org/10.1038/nn.4641

Moron, J. A., Perez, V., Pasto, M., Lizcano, J. M., & Unzeta, M. (2000). FA-70, a novel selective and irreversible monoamine oxidase-A inhibitor: Effect on monoamine metabolism in mouse cerebral cortex. *Journal of Pharmacology and Experimental Therapeutics*, *292*, 788–794.

Mosharov, E. V., Larsen, K. E., Kanter, E., Phillips, K. A., Wilson, K., Schmitz, Y., Krantz, D. E., Kobayashi, K., Edwards, R. H., & Sulzer, D. (2009). Interplay between cytosolic dopamine, calcium, and α-synuclein causes selective death of substantia nigra neurons. *Neuron*, *62*(2), 218–229. https://doi.org/10.1016/j.neuron.2009.01.033

Norris, E. H., & Giasson, B. I. (2005). Role of oxidative damage in protein aggregation associated with Parkinson's disease and related disorders. *Antioxidants & Redox Signaling*, *7*, 672–684. https://doi.org/10.1089/ars.2005.7.672

Norris, E. H., Giasson, B. I., Hodara, R., Xu, S., Trojanowski, J. Q., Ischiropoulos, H., & Lee, V. M. (2005). Reversible inhibition of alpha-synuclein fibrillization by dopaminochrome-mediated conformational alterations. *Journal of Biological Chemistry*, *280*, 21212–21219.

Panneton, W. M., Kumar, V. B., Gan, Q., Burke, W. J., & Galvin, J. E. (2010). The neurotoxicity of DOPAL: Behavioral and stereological evidence

for its role in Parkinson disease pathogenesis. *PLoS One*, *5*, e15251. https://doi.org/10.1371/journal.pone.0015251

Park, H.-J., Lee, K.-W., Park, E. S., Oh, S., Yan, R., Zhang, J., Beach, T. G., Adler, C. H., Voronkov, M., Braithwaite, S. P., Stock, J. B., & Mouradian, M. M. (2016). Dysregulation of protein phosphatase 2A in parkinson disease and dementia with lewy bodies. *Annals of Clinical and Translational Neurology*, *3*, 769–780. https://doi.org/10.1002/acn3.337

Park, S. S., Schulz, E. M., & Lee, D. (2007). Disruption of dopamine homeostasis underlies selective neurodegeneration mediated by alpha-synuclein. *European Journal of Neuroscience*, *26*, 3104–3112.

Peng, X., Tehranian, R., Dietrich, P., Stefanis, L., & Perez, R. G. (2005). Alpha-synuclein activation of protein phosphatase 2A reduces tyrosine hydroxylase phosphorylation in dopaminergic cells. *Journal of Cell Science*, *118*, 3523–3530.

Perez, R. G., Waymire, J. C., Lin, E., Liu, J. J., Guo, F., & Zigmond, M. J. (2002). A role for alpha-synuclein in the regulation of dopamine biosynthesis. *Journal of Neuroscience*, *22*, 3090–3099.

Pfaffl, M. W. (2001). A new mathematical model for relative quantification in real-time RT-PCR. *Nucleic Acids Research*, *29*, e45. https://doi.org/10.1093/nar/29.9.e45

Pifl, C., Rajput, A., Reither, H., Blesa, J., Cavada, C., Obeso, J. A., Rajput, A. H., & Hornykiewicz, O. (2014). Is Parkinson's disease a vesicular dopamine storage disorder? Evidence from a study in isolated synaptic vesicles of human and nonhuman primate striatum. *Journal of Neuroscience*, *34*, 8210–8218. https://doi.org/10.1523/JNEUROSCI.5456-13.2014

Ploteghe, N., Berti, G., Ferrari, E., Tessari, I., Zanetti, M., Lunelli, L., Greggio, E., Bisaglia, M., Veronesi, M., Girotto, S., Dalla Serra, M., Perego, C., Casella, L., & Bubacco, L. (2017). DOPAL derived alpha-synuclein oligomers impair synaptic vesicles physiological function. *Scientific Reports*, *7*, 40699. https://doi.org/10.1038/srep40699

Puspita, L., Chung, S. Y., & Shim, J. W. (2017). Oxidative stress and cellular pathologies in Parkinson's disease. *Molecular Brain*, *10*, 53. https://doi.org/10.1186/s13041-017-0340-9

Qu, J., Yan, H., Zheng, Y., Xue, F., Zheng, Y., Fang, H., Chang, Y., Yang, H., & Zhang, J. (2018). The molecular mechanism of alpha-synuclein dependent regulation of protein phosphatase 2A activity. *Cellular Physiology and Biochemistry: International Journal of Experimental Cellular Physiology, Biochemistry, and Pharmacology*, *47*, 2613–2625. https://doi.org/10.1159/000491657

Ricke, K. M., Paß, T., Kimoloi, S., Fährmann, K., Jüngst, C., Schauss, A., Baris, O. R., Aradjanski, M., Trifunovic, A., Eriksson Faelker, T. M., Bergami, M., & Wiesner, R. J. (2020). Mitochondrial dysfunction combined with high calcium load leads to impaired antioxidant defense underlying the selective loss of nigral dopaminergic neurons. *Journal of Neuroscience*, *40*, 1975–1986. https://doi.org/10.1523/JNEUROSCI.1345-19.2019

Salahpour, A., Ramsey, A. J., Medvedev, I. O., Kile, B., Sotnikova, T. D., Holmstrand, E., Ghisi, V., Nicholls, P. J., Wong, L., Murphy, K., Sesack, S. R., Wightman, R. M., Gainetdinov, R. R., & Caron, M. G. (2008). Increased amphetamine-induced hyperactivity and reward in mice overexpressing the dopamine transporter. *Proceedings of the National Academy of Sciences*, *105*, 4405–4410. https://doi.org/10.1073/pnas.0707646105

Salvatore, M. F. (2014). ser31 Tyrosine hydroxylase phosphorylation parallels differences in dopamine recovery in nigrostriatal pathway following 6-OHDA lesion. *Journal of Neurochemistry*, *129*, 548–558. https://doi.org/10.1111/jnc.12652

Salvatore, M. F., Calipari, E. S., & Jones, S. R. (2016). Regulation of tyrosine hydroxylase expression and phosphorylation in dopamine transporter-deficient mice. *ACS Chemical Neuroscience*, *7*(7), 941–951. https://doi.org/10.1021/acschemneuro.6b00064

Salvatore, M. F., Nejtek, V. A., & Khoshbouei, H. (2018). Prolonged increase in ser31 tyrosine hydroxylase phosphorylation in substantia nigra following cessation of chronic methamphetamine. *Neurotoxicology*, *67*, 121–128. https://doi.org/10.1016/j.neuro.2018.05.003

Salvatore, M. F., Waymire, J. C., & Haycock, J. W. (2001). Depolarization-stimulated catecholamine biosynthesis: Involvement of protein kinases and tyrosine hydroxylase phosphorylation sites in situ. *Journal of Neurochemistry*, *79*, 349–360. https://doi.org/10.1046/j.1471-4159.2001.00593.x

Sarafian, T. A., Yacoub, A., Kunz, A., Aranki, B., Serobyan, G., Cohn, W., Whitelegge, J. P., & Watson, J. B. (2019). Enhanced mitochondrial inhibition by 3,4-dihydroxyphenyl-acetaldehyde (DOPAL)-oligomerized alpha-synuclein. *Journal of Neuroscience Research*, *97*, 1689–1705.

Schmittgen, T. D., & Livak, K. J. (2008). Analyzing real-time PCR data by the comparative C(T) method. *Nature Protocols*, *3*, 1101–1108. https://doi.org/10.1038/nprot.2008.73

Segura-Aguilar, J., Paris, I., Munoz, P., Ferrari, E., Zecca, L., & Zucca, F. A. (2014). Protective and toxic roles of dopamine in Parkinson's disease. *Journal of Neurochemistry*, *129*, 898–915. https://doi.org/10.1111/jnc.12686

Shepherd, C. T., Moran Lauter, A. N., & Scott, M. P. (2009). Determination of transgene copy number by real-time quantitative PCR. *Methods in Molecular Biology*, *526*, 129–134.

Spina, M. B., & Cohen, G. (1989). Dopamine turnover and glutathione oxidation: Implications for Parkinson disease. *Proceedings of the National Academy of Sciences*, *86*, 1398–1400. https://doi.org/10.1073/pnas.86.4.1398

Stansley, B. J., & Yamamoto, B. K. (2013). L-dopa-induced dopamine synthesis and oxidative stress in serotonergic cells. *Neuropharmacology*, *67*, 243–251. https://doi.org/10.1016/j.neuropharm.2012.11.010

Storch, A., Ott, S., Hwang, Y.-I., Ortmann, R., Hein, A., Frenzel, S., Matsubara, K., Ohta, S., Wolf, H.-U., & Schwarz, J. (2002). Selective dopaminergic neurotoxicity of isoquinoline derivatives related to Parkinson's disease: Studies using heterologous expression systems of the dopamine transporter. *Biochemical Pharmacology*, *63*, 909–920. https://doi.org/10.1016/S0006-2952(01)00922-4

Sulzer, D., Chen, T. K., Lau, Y. Y., Kristensen, H., Rayport, S., & Ewing, A. (1995). Amphetamine redistributes dopamine from synaptic vesicles to the cytosol and promotes reverse transport. *Journal of Neuroscience*, *15*, 4102–4108. https://doi.org/10.1523/JNEUROSCI.15-05-04102.1995

Surmeier, D. J. (2007). Calcium, ageing, and neuronal vulnerability in Parkinson's disease. *The Lancet Neurology*, *6*, 933–938. https://doi.org/10.1016/S1474-4422(07)70246-6

Surmeier, D. J. (2018). Determinants of dopaminergic neuron loss in Parkinson's disease. *The FEBS Journal*, *285*, 3657–3668. https://doi.org/10.1111/febs.14607

Surmeier, D. J., Obeso, J. A., & Halliday, G. M. (2017). Selective neuronal vulnerability in Parkinson disease. *Nature Reviews Neuroscience*, *18*, 101–113. https://doi.org/10.1038/nrn.2016.178

Takahashi, N., Miner, L. L., Sora, I., Ujike, H., Revay, R. S., Kostic, V., Jackson-Lewis, V., Przedborski, S., & Uhl, G. R. (1997). VMAT2 knockout mice: Heterozygotes display reduced amphetamine-conditioned reward, enhanced amphetamine locomotion, and enhanced MPTP toxicity. *Proceedings of the National Academy of Sciences*, *94*, 9938–9943. https://doi.org/10.1073/pnas.94.18.9938

Taylor, T. N., Alter, S. P., Wang, M., Goldstein, D. S., & Miller, G. W. (2014). Reduced vesicular storage of catecholamines causes progressive degeneration in the locus ceruleus. *Neuropharmacology 76 Pt A*, 97–105. https://doi.org/10.1016/j.neuropharm.2013.08.033

Taylor, T. N., Caudle, W. M., Shepherd, K. R., Noorian, A., Jackson, C. R., Iuvone, P. M., Weinshenker, D., Greene, J. G., & Miller, G. W. (2009). Nonmotor symptoms of Parkinson's disease revealed in an animal model with reduced monoamine storage capacity. *Journal of Neuroscience*, *29*, 8103–8113. https://doi.org/10.1523/JNEUROSCI.1495-09.2009

Tian, H., Lu, Y., Liu, J., Liu, W., Lu, L., Duan, C., Gao, G., & Yang, H. (2018). Leucine carboxyl methyltransferase downregulation and protein phosphatase methylesterase upregulation contribute toward the inhibition of protein phosphatase 2A by alpha-synuclein. *Frontiers in Aging Neuroscience*, *10*, 173.

Vecchio, L. M., Bermejo, M. K., Beerepoot, P., Ramsey, A. J., & Salahpour, A. (2014). N-terminal tagging of the dopamine transporter impairs protein expression and trafficking in vivo. *Molecular and Cellular Neurosciences*, *61*, 123–132. https://doi.org/10.1016/j.mcn.2014.05.007

Vernon, A. C. (2009). Mice with reduced vesicular monoamine storage content display nonmotor features of Parkinson's disease. *Journal of Neuroscience*, *29*, 12842–12844. https://doi.org/10.1523/JNEUROSCI.4156-09.2009

Walker, D. G., Lue, L.-F., Adler, C. H., Shill, H. A., Caviness, J. N., Sabbagh, M. N., Akiyama, H., Serrano, G. E., Sue, L. I., & Beach, T. G. (2013). Changes in properties of serine 129 phosphorylated α-synuclein with progression of Lewy-type histopathology in human brains. *Experimental Neurology*, *240*, 190–204. https://doi.org/10.1016/j.expneurol.2012.11.020

Werner-Allen, J. W., Levine, R. L., & Bax, A. (2017). Superoxide is the critical driver of DOPAL autoxidation, lysyl adduct formation, and crosslinking of alpha-synuclein. *Biochemical and Biophysical Research Communications*, *487*, 281–286.

Wey, M. C., Fernandez, E., Martinez, P. A., Sullivan, P., Goldstein, D. S., & Strong, R. (2012). Neurodegeneration and motor dysfunction in mice lacking cytosolic and mitochondrial aldehyde dehydrogenases: Implications for Parkinson's disease. *PLoS One*, *7*, e31522. https://doi.org/10.1371/journal.pone.0031522

Wu, B., Liu, Q., Duan, C., Li, Y., Yu, S., Chan, P., Ueda, K., & Yang, H. (2011). Phosphorylation of alpha-synuclein upregulates tyrosine hydroxylase activity in MN9D cells. *Acta Histochemica*, *113*, 32–35.

Zhou, J., Broe, M., Huang, Y., Anderson, J. P., Gai, W.-P., Milward, E. A., Porritt, M., Howells, D., Hughes, A. J., Wang, X., Halliday, G. M. (2011). Changes in the solubility and phosphorylation of α-synuclein over the course of Parkinson's disease. *Acta Neuropathologica*, *121*(6), 695–704. https://doi.org/10.1007/s00401-011-0815-1

SUPPORTING INFORMATION

Additional supporting information may be found online in the Supporting Information section.